NASA TECHNICAL MEMORANDUM

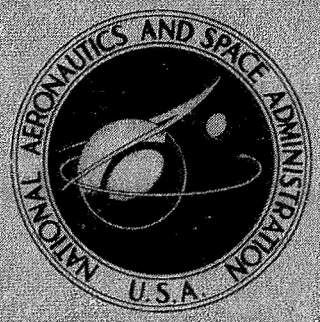

NASA TM X-2461

NASA TM X-2461

HYDROGEN PLASMA TESTS OF SOME INSULATING COATING SYSTEMS FOR THE NUCLEAR ROCKET THRUST CHAMBER

by Arthur N. Curren, Salvatore J. Grisaffe, and Kurt C. Wycoff

Lewis Research Center
Cleveland, Ohio 44135

NATIONAL AERONAUTICS AND SPACE ADMINISTRATION • WASHINGTON, D. C. • JANUARY 1972

1. Report No.	2. Government Accession No.	3. Recipient's Catalog No.
NASA TM X-2461		

4. Title and Subtitle	5. Report Date
HYDROGEN PLASMA TESTS OF SOME INSULATING COATING SYSTEMS FOR THE NUCLEAR ROCKET THRUST CHAMBER	January 1972
	6. Performing Organization Code
7. Author(s)	8. Performing Organization Report No.
Arthur N. Curren, Salvatore J. Grisaffe, and Kurt C. Wycoff	E-6565
	10. Work Unit No.
	112-29
9. Performing Organization Name and Address	11. Contract or Grant No.
Lewis Research Center National Aeronautics and Space Administration Cleveland, Ohio 44135	
	13. Type of Report and Period Covered
12. Sponsoring Agency Name and Address	Technical Memorandum
National Aeronautics and Space Administration Washington, D.C. 20546	14. Sponsoring Agency Code

15. Supplementary Notes

16. Abstract

Several plasma-sprayed and slurry-coated insulating coating systems were evaluated for structural stability in a low-pressure hot hydrogen environment at a maximum heat flux of 19.6×10^{6} W/m^{2} (12 Btu/(in.^{2})(sec)). The heat was provided by an electric-arc plasma generator. The coating systems consisted of a number of thin (0.051×10^{-3} to 0.508×10^{-3} m (0.002 to 0.020 in.)) layers of metal oxides and/or metals. The materials included molybdenum, nichrome, tungsten, alumina, zirconia, and chromia. The study indicates potential usefulness in this environment for some coatings and points up the need for improved coating application techniques.

17. Key Words (Suggested by Author(s))	18. Distribution Statement
Nuclear rocket Rocket coatings Ceramic coatings Thermal insulation Environment simulation	Unclassified - unlimited

19. Security Classif. (of this report)	20. Security Classif. (of this page)	21. No. of Pages	22. Price*
Unclassified	Unclassified	55	$3.00

* For sale by the National Technical Information Service, Springfield, Virginia 22151

HYDROGEN PLASMA TESTS OF SOME INSULATING COATING SYSTEMS FOR THE NUCLEAR ROCKET THRUST CHAMBER

by Arthur N. Curren, Salvatore J. Grisaffe, and Kurt C. Wycoff

Lewis Research Center

SUMMARY

An experimental investigation was conducted to evaluate a number of contractor-fabricated thermal-insulating coating systems for their structural stability in a hot hydrogen environment. The maximum imposed heat-flux level was 19.6×10^{6} watts/meter^2 (12 Btu/(in.^{2})(sec)) through the coating system, and the heat was supplied by means of an electric-arc plasma generator at an environment pressure of about 1.4×10^{4} newtons/meter^2 absolute (2 psia).

The coating systems were composed of a number of relatively thin (0.051×10^{-3} to 0.508×10^{-3} m (0.002 to 0.020 in.)) layers of metal oxides and/or metals. The metals included molybdenum, nichrome, and tungsten; and the oxides included alumina, zirconia, and chromia. The coating systems were all either plasma sprayed or slurry coated and cured in place.

The testing was done in two modes: step testing at consecutively higher heat-flux levels to determine the maximum level of structural stability, and duration testing for a total of 30 minutes at 19.6×10^{6} watts/meter^2 (12 Btu/(in.^{2})(sec)) to determine structural stability over a longer time period. Results of the tests indicate that a relatively thick tungsten-rich coating system performed best on the basis of coating loss and that an alumina-nichrome graded coating with a zirconia overlay shows promise for minimizing depth of surface cracking and coating loss. In general, the study points up the need for improved coating application control techniques.

INTRODUCTION

Current requirements for regeneratively cooled nuclear rocket thrust chambers for space application involve relatively long periods (hours) of operation with wall surface temperatures near the maximum design limit for the structural materials (stainless

steels) being considered. The resulting high temperature gradients give rise to high wall stress levels and limit thrust chamber cyclic life. As specific impulse requirements for the nuclear rocket are inevitably upgraded, the resulting increase in heat flux and wall temperature levels will approach or exceed the practical limits of regenerative-cooling capability and will further reduce chamber cyclic life. To accommodate this higher-performance operation, an effective method for reducing the heat flux to the chamber wall will be required. Thermal-insulating coatings are a potential solution to this problem, as indicated in reference 1. If a suitable thickness of material having low thermal conductivity can be bonded to the hot-gas side of the chamber wall, the wall heat flux and the metal interface temperature levels can be reduced by virtue of the low thermal conductivity and the resulting high coating-surface temperature. The heat-flux reduction can be 50 percent or more, depending on the coating material and the thrust chamber operating conditions.

Experience with some simple coatings applied to chemical rocket thrust chambers indicates the need for further development of this method for thermal protection. In a number of early programs, failure of rocket thrust chamber coatings by cracking, flaking, and spalling was common. To prevent these kinds of failures, the "graded" coating system concept has evolved (ref. 2). Such thermal barriers are herein termed "systems" since they are composed of more than one layer and generally the layers are composed of more than one material. Reference 2 provides evidence of the superiority of the graded coating system over a simple one-component coating from the standpoint of structural stability during testing in a chemical (liquid oxygen - liquid ammonia) rocket engine. A graded coating system is probably best described as a coating of metal and ceramic in which the composition is varied in a layer-upon-layer manner from a metal-rich mixture at the surface to be protected to a ceramic-rich mixture at the surface exposed to the hot gases. By this method, according to reference 2, the problem of weak, sensitive interfaces between metal and ceramic is reduced. Further, this structuring can avoid relatively thick layers of any one composition and ideally allows for the control of relative thermal expansion between pairs of adjacent layers for the most severe imposed temperature gradient, so that critical shear stress levels are not exceeded. With some exceptions, the layers are so arranged that the material with the largest thermal expansion coefficient is adjacent to the thrust chamber wall, while the material with the lowest expansion coefficient is exposed to the hot gas in the thrust chamber.

The purpose of this investigation was to examine a number of graded coating systems for their structural stability in a simulated nuclear rocket thrust chamber environment as a first step in the development of effective coating systems for nuclear rocket applications. Eight different coating system types were applied to sample pieces which simulated sections of a cooled rocket thrust chamber wall. A total of five contractors supplied three samples of each coating system assigned to them, and some types were

supplied by more than one contractor. In all, 51 coating sample pieces were involved in the evaluation program. The ingredients of the coating systems examined in this study were limited to selected metals and metal oxides. Included in these materials were molybdenum, nichrome, tungsten, alumina, zirconia, and chromia. The coating systems were specified primarily on the basis of material property estimates, some empirical data, and compatibility judgments.

The coating systems examined were subjected to a maximum heat flux of 19.6×10^6 watts/meter^2 (12 Btu/(in.^{2})(sec)) for a maximum of 30 minutes accumulated time. This heat-flux level and time period were considered representative of actual nuclear rocket application and were compatible with the test facility. The samples were tested with a relatively uniformly heated area of about 2.54×10^{-2} meter (1.0 in.) in diameter. The heat was applied by means of a 200-kilowatt (maximum) electric-arc plasma generator which produced a hydrogen plasma stream in a low-pressure environment (about 1.4×10^4 N/m^2 abs, or 2.0 psia). The coating sample surface was oriented perpendicularly to the plasma stream, resulting in a directly impinging plasma flow. This low-pressure environment and directly impinging flow is, of course, different from the conditions which would be encountered by a coating on a nuclear rocket thrust chamber wall. In spite of these differences, however, these tests should provide meaningful screening information valuable to the development of coating systems for the actual application. The testing-caused structural changes of the coating systems were evaluated by means of direct observations, microscopic section analysis, and X-ray diffraction techniques. The results of these examinations are noted herein, as well as the possible implications for coating systems for actual nuclear thrust chamber applications.

This report displays all values in the International System of Units (SI) as the primary system. U. S. Customary Units also appear as a secondary system after the SI values, in parentheses. The basic measurements and calculations for this study were made in U. S. Customary Units.

COATING SYSTEMS

The coating systems selected for evaluation in this study were composed of materials commonly considered for thermal-insulating coatings in a high-temperature reducing environment. These materials include tungsten, alumina, zirconia, hafnia, and chromia. Other materials used were included for their anticipated value in enhancing component binding and oxide adherence to the substrate and for their expected influence on the thermal expansion characteristics of mixtures with the oxides. These materials were nichrome, molybdenum, nickel, copper, and a gold-based brazing alloy. In table I, details of the specific coating systems are given. Types 1, 3, 4, 5, and 6 were specified to the contractors for fabrication; types 2, 7, and 8 were suggested by the

contractors as having potential value for this application. The requested types, except type 6, were supplied by more than one contractor each; and three samples of each coating system were fabricated. In all, a total of 51 samples were supplied. While the testing heat-flux level, 19.6×10^6 watts/meter^2 (12 Btu/(in.^{2})(sec)), and a substrate-coating system interface temperature of about 811 K (1460° R) was implied to the contractors, a general lack of information as to the properties of the as-applied coating materials permitted only very rough estimates as to proper coating thicknesses. Essentially, the coating systems layer compositions and thicknesses were specified primarily on the basis of property estimates, some empirical data, and compatibility judgments. All the contractors except E (see table I) applied the coating systems by arc plasma spraying; contractor E used the slurry-coat application method, with curing in place.

Briefly, in the plasma-spray method, the coating material in fine powdered form is mixed with and carried by a vehicle gas through an accelerating nozzle across which a high-energy electric arc is established. The arc heats the flowing mixture so that the powder component is at least partially melted. The high-velocity powder particles are then directed to the object to be coated and the colliding particles resolidify and adhere to the object. In the slurry-coating method, a wet mixture of finely ground coating material and a binding agent such as phosphoric acid is applied to the object to be coated in the desired thickness by troweling or air spraying. The coating material then is heated to "cure," or dry out, the coating.

The contractors were not required to report all details concerning their coating application process (equipment, environment used, etc.). As a consequence, that information is not available to present in this report.

APPARATUS AND EQUIPMENT

Sample Piece and Heat-Flux Meter

Configuration details of the sample pieces to which all the coating systems were applied are shown in figure 1(a). The base block, of type 304 stainless steel, is formed to support three brazed-in-place adjacent parallel tubes whose shells are fabricated of 0.305×10^{-3}-meter (0.012-in.) thick type 347 stainless steel. The block also contains access ports for tube coolant (water) supply and provision for instrumentation for the heat-flux-meter version of the sample piece. Figure 1(b) illustrates the ideal appearance of the cross section of the center sample-piece tube in the testing area with a coating system (in this case, type 1) applied. It should be noted that the sample piece used for this function has no instrumentation. The tube size is considered reasonably representative of the general size anticipated in the high-heat-flux portions of a nuclear rocket thrust chamber. The tube-to-base attachment technique, however, was selected only on

the basis of convenience for this study. The heat-flux-meter version of the sample piece, whose function is detailed in a later section of the study, is shown in cross section in figure 1(c). It is seen that a very small diameter (0.254×10^{-3} m (0.010 in.)) thermocouple assembly is embedded in the tube wall with its sensing junction located at the tube crown. Actually, each heat-flux meter had two such thermocouples located in close proximity (note thermocouple access holes shown in fig. 1(a)) for redundancy. Details of the fabrication of the heat-flux meters are discussed in appendix A.

Test Facility

The heat to the coating system sample was supplied by means of an electric-arc plasma generator which produces a hydrogen plasma plume, or stream. The plasma generator, the coating system sample, and the heat-flux meter were all contained in a closed vessel, the internal environment and pressure level of which were controllable. The facility is illustrated schematically in figure 2. The coating system sample piece, the heat-flux meter, and the plasma generator were all cooled with distilled water to avoid mineral deposits on internal surfaces. An externally controlled component-positioning mechanism is an important feature of the facility. This device has three degrees of freedom - that is, it can vary the plasma-generator-to-sample (or to heat-flux meter) distance as well as the vertical and horizontal sample and heat-flux-meter positions. Figure 3 presents a cutaway view of the containment vessel interior. The sample piece and the heat-flux meter are laterally surrounded with a water-cooled shield which protects the positioning mechanism and posterior instrument lines from heating damage during testing. Observation ports in the containment vessel permit closed-circuit television test monitoring and direct visual examination of the sample coating system between test periods without having to open the vessel.

Plasma Generator

The hydrogen plasma generator used to heat the coating systems in this study is a larger modified version of the general type of apparatus used to coat the samples. A schematic of this apparatus appears in figure 4. In the heating plasma generator, a stream of hydrogen is passed through an accelerating nozzle across which an electric arc is established. The arc heats the flowing stream to extremely high temperatures; and the gas becomes partially ionized, or a "plasma" stream. The plasma stream is directed to the object to be heated. The manufacturer of the plasma generator used in this study indicates the plasma-stream core temperature to be about 11 100 K (20 000° R) at electrical input power levels considerably lower than those generally used in this in-

vestigation, but at about the same hydrogen flow rates. The generator here operates in an oxidant-free environment, so combustion of the hydrogen does not occur. The generator has an integral water-cooling system which protects the cables, the fittings, and the housing as well as the nozzle components. The construction of the generator used here prevented the installation of instrumentation at the nozzle entrance, but from calculated pressure losses from a known near upstream condition, the hydrogen pressure at the nozzle inlet was estimated to be about 51.7×10^4 newtons/meter^2 absolute (75 psia). The input electrical power required to produce a desired heat flux to the coating system sample for a fixed hydrogen flow rate and generator-to-sample spacing (0.273×10^{-3} kg/sec (0.0006 lbm/sec) and 8.88×10^{-2} m (3.5 in.), respectively) was found to be a variable, depending on nozzle condition and other factors. The maximum power required to produce the desired heat-flux level of 19.6×10^6 watts/meter^2 (12 Btu/(in.^{2})(sec)) was 112 kilowatts (800 A, 140 V) and the mean was about 90 kilowatts (600 A, 150 V), direct current. Both the power supply and the generator are estimated to have maximum power operating levels in testing mode of about 200 kilowatts. The power supply no-load voltage is 200 volts. Additional operating characteristics of the plasma generator are described in a later section of this report, General Operating Procedures.

Flowmeters, Controls, and Instruments

Cooling water flow rates to the sample, the heat-flux meter, and the plasma generator were measured by means of turbine meters, while supply pressure was measured by means of an electrical transducer. Additionally, the heat-flux-meter water pressure was separately measured by a Bourdon-tube gage. Iron-constantan thermocouples were employed to measure coolant temperature at the plasma generator, the sample piece, and the heat-flux-meter inlet and outlet fittings. The hydrogen and purging nitrogen and helium flow rates were measured by rotameters, and the supply pressures were measured with both an electrical transducer and a Bourdon-tube gage for redundancy. Alternating-current electrical power to the plasma generator power supplies was regulated by means of a variable ratio transformer, and the direct current supplied to the plasma generator was monitored with a voltmeter and an ammeter. In addition, a wattmeter provided a direct electrical power reading and was continuously traced on a recording potentiometer. The recording potentiometer also continuously recorded the readouts of the heat-flux-meter Chromel-Alumel thermocouples.

COATING SYSTEM SAMPLE TESTING CONSIDERATIONS

To test the coating system samples at known conditions, a method to determine the actual heat flux at the sample was required. The time and expense required to suitably instrument each coating system sample piece precluded that approach. Rather, it was decided to employ a separate instrument for heat-flux measurement at the sample testing position. With this method, an arrangement was required to remotely accomplish the interchange of the positions of the coating system sample piece and the heat-flux meter within the containment vessel. For that purpose, and for other anticipated component manipulation needs, a positioning mechanism was designed, fabricated, and installed in the containment vessel. The mechanism is indicated in figure 3. In use, the electrical power input, gas flow rate, etc., to the plasma generator were adjusted with the plasma stream impinging on the heat-flux meter. When the desired stable testing heat flux was established, the heat-flux meter was withdrawn and the sample was substituted in the heated position. While the use of such short-term "calibrations" are quite useful, it was found that attempts to establish a permanent calibration could give rise to significant errors. Apparently, relatively minor changes in electrode geometry, containment vessel pressure, and other conditions normally occurring over a longer time period (several minutes or hours) can cause large changes in the sample heat-flux level for identical power input and gas flow levels. The heat-flux meter was reinserted into the plasma stream at the end of the sample heating period to verify that the desired heating level had been maintained. Heat-flux variations during the test period not exceeding ± 0.82 watt/meter^2 (0.5 Btu/(in.^{2})(sec)) were considered acceptable. The tests performed for this investigation did not exceed this heat-flux variation, which corresponds to a heat-flux-meter measured temperature variation not exceeding ± 11.1 K ($\pm 20^\circ$ R). For those heat-flux meters on which the two adjacent thermocouples displayed measurably different temperatures, the discrepancy never exceeded 11.1 K (20° R). Where temperature reading differences between the two thermocouples existed, the higher temperature was assumed to be the correct one.

The heat-flux meter itself, as indicated earlier, is an instrumented version of the coating system sample piece, as is shown in figure 1(c). This heat-flux meter has the obvious advantage of having the same configuration as the coating system sample piece, except for the coating system itself.

For even more complete simulation, the coolant supply weight flow rate and pressure to the heat-flux meter and sample piece were maintained at identical levels. The method for determining the heat flux through the coating system sample by means of the heat-flux meter used in this study is detailed in appendix B.

Heat-Flux-Meter and Sample Heat-Flux Comparisons

As described earlier, the heat flux desired for coating system sample testing was established with a heat-flux meter in the heating position in the test facility. Following that, the heat-flux meter was quickly withdrawn and replaced (within 5 sec) with the coated sample. Since the samples are protected with a coating system and the calorimeters are not, one would conclude that the heat flux to the sample must be less than that to the heat-flux meter. While that is certainly true, one of the basic assumptions made for this study is that the differences in heat flux between the sample and the heat-flux meter is insignificantly small. The justification of this assumption is the extremely high plasma stream temperature and enthalpy. With such very high stream temperature and enthalpy levels, the heat flux is not changed significantly by the relatively small difference between the sample coating system and heat-flux-meter surface temperatures. Some experiments were performed which demonstrated that the assumption is satisfactorily accurate. One of these experiments, with typical results, is described in the next paragraph.

A heat-flux meter was coated with a system typical of those considered in this study (see fig. 5). The plasma spraying was done at the Lewis Research Center. Both the coated heat-flux meter and an identical, but uncoated, heat-flux meter were installed in the test facility and alternately heated through a series of identical heat-flux levels to 19.6×10^6 watts/meter^2 (12 Btu/(in.^{2})(sec)), noting the electrical power levels required for each step. The resulting comparison data are shown in figure 5 and support the previously stated assumption of the heat-flux relation between the sample and the heat-flux meter. The heat flux to the coated and uncoated heat-flux meters was equal for equal plasma generator electrical power levels, considering estimated data precision. Of course, the validity of the assumption is limited to coating materials and thicknesses similar to those considered in this study. The precision with which the same heat flux was established for this study is estimated to be within ±10 percent at all values from 0 to 19.6×10^6 watts/meter^2 (12 Btu/(in.^{2})(sec)).

Heat-Flux-Meter Heated Area

The hydrogen plasma stream heats only a small part of the coating system sample piece or heat-flux meter. The heated area is essentially circular and centers on the middle coolant tube crown at the midpoint of the longitudinal centerline. To produce valid test results, it is apparent that a suitably sized area of the coating surface must be heated relatively uniformly. No guidelines exist for such a heated-area requirement, but for this study an area enclosed by a circle having a diameter of at least 10 times the coating thickness of the coating system being tested and having a center-to-edge heat-

flux falloff not exceeding 25 percent was chosen as a goal. Such a requirement would ensure that the heated area would be larger in dimension than the distance between adjacent cracks in the surface crack patterns commonly seen in some coating samples tested in the early phases of this investigation. A heated testing area with dimensions smaller than those of the crack pattern might give rise to misleading results.

By means of the component-positioning mechanism in the test facility, a number of temperature surveys were made to examine the heat-flux distribution near the center (maximum heat-flux point) of the heated area. In a series of short displacements, starting from center in the plasma stream, the heat-flux meter was moved perpendicular to the plasma stream. At each station, the heat flux was recorded. In separate steps, data were taken for both longitudinal and lateral profiles. Only a very limited lateral survey could be made because of the danger of damaging the nearby uncooled edge of the heat-flux meter. Figure 6 presents the results of one of the surveys which is typical of all of them. In the survey results shown, the heat flux fell from 19.94×10^6 watts/meter^2 (12.2 Btu/(in.^{2})(sec)) at the center to about 17.0×10^6 watts/meter^2 (10.38 Btu/(in.^{2})(sec)) at a radius of about 7.62×10^{-3} meter (0.3 in.). The distribution indicates that for the thickest coating system tested, which was 0.61×10^{-3} meter (0.024 in.) thick (type 6 in table I), the heat flux was uniform within 15 percent over a diameter of about 25 coating system thicknesses. Obviously, this heat-flux distribution was well within the minimum standard pattern desired for this study.

EXPERIMENTAL PROCEDURES

Each coating system sample investigated in this study was subjected to a uniform series of examinations before and after the hot-testing sequences. A strong effort was made to process each sample similarly to make final evaluations and comparisons of the systems reliable. The following paragraphs describe these examinations, along with pretest conditioning and the hot-testing procedures, in chronological order. In addition, a summary of the entire experimental procedure is presented in table II.

Sample Pretest Examinations

Two of the three coating system sample pieces of each vendor's type (see table I) were selected for testing. The third sample was reserved for possible later retesting to confirm unusual results or for backup in case of an accident to one of the other two samples. The two selected sample pieces were full-view color photographed for record of general appearance, and closeup monochrome photographs (about ×3 magnification) were made of the central testing area for the same purpose. In addition, detailed visual

microscopic examinations were made of the tested area of the sample to make note of surface texture appearance, particle distribution, color, and other pertinent characteristics. Finally, coating system scrapings were taken from the tube-end regions of the sample pieces for later crystal form comparison (by use of X-ray diffraction techniques) with scrapings taken from the tested area of the sample.

Sample Cold-Shock Conditioning

In order to simulate the rapid temperature drop from ambient to cryogenic temperature levels of a regeneratively cooled thrust chamber wall, each coating system sample piece was cold shocked prior to hot testing. This conditioning was accomplished by rapidly (within several seconds) gravity filling the sample-piece cooling tubes with liquid nitrogen (77.75 K (140° R)) at open room conditions. The sample piece was then allowed to return to ambient temperature at open room conditions. Following that, a visual microscopic inspection was again made of the sample's testing area. No significant changes due to the cold-shock conditioning were noted.

Sample Hot Testing

Hot testing of the coating system sample pieces was accomplished in two separate modes. One of the two selected coating system samples of each vendor's types was "step tested" and the second was "endurance tested." Each of these testing modes is detailed in the following paragraphs. In both testing sequences, the coating system sample piece was "conditioned" at the testing environment before the initiation of hot testing. This conditioning consisted of thoroughly purging the facility containment vessel interior with nitrogen and reducing the pressure to about 1.4×10^{4} newtons/meter^2 absolute (2 psia). The purging procedure eliminates oxygen from the containment vessel to ensure a reducing environment and to prevent combustion of the hydrogen plasma. The low-pressure condition was maintained for a minimum of 15 minutes before hot testing was started. This procedure was intended to effectively purge the porous coating system structure of trapped air and/or moisture and to equalize the pressure in any internal voids. If it became necessary to open the containment vessel before the testing of a particular sample was complete, the purging and low-pressure conditioning routines were repeated before testing was resumed.

Step testing. - This testing mode was intended to closely identify the heat-flux level at or below 19.6×10^{6} watts/meter^2 (12 Btu/(in.^{2})(sec)), where a coating system might structurally fail in a short time. In it, the sample was heated in hydrogen plasma, in 30-second intervals, at progressively higher heat-flux levels, until failure occurred or

19.6×10^6 watts/meter^2 (12 Btu/(in.^{2})(sec)) was reached. The testing started at 1.635×10^6 watts/meter^2 (1 Btu/(in.^{2})(sec)) and was increased by 1.635×10^6 watts/meter^2 (1 Btu/(in.^{2})(sec)) in each succeeding test period. The samples were visually inspected between each testing period by means of the observation ports in the containment vessel shown in figure 3.

Endurance testing. - After a coating system had demonstrated at least short-term structural stability at 19.6×10^6 watts/meter^2 (12 Btu/(in.^{2})(sec)) in the step-testing sequences, it was subjected to an endurance-testing procedure. The purpose of this test was to determine the structural stability of the coating system for a longer time at this heat-flux level. Consequently, the endurance-testing procedure was to subject the coating system to a heat flux of 19.6×10^6 watts/meter^2 (12 Btu/(in.^{2})(sec)) in hydrogen plasma for a total time of 30 minutes. As was indicated earlier, this heat-flux level and time period are considered reasonably representative of an actual nuclear rocket application and are compatible with the test facility. The testing was done in several discrete time periods, none exceeding 5 minutes. After each testing period, the condition of the coating system was noted by visual examination by means of the observation ports in the containment vessel.

Sample Post-Test Examinations

As with the earlier pretest examinations, the coating system samples were subjected to a uniform series of examinations after they were hot tested. Extreme care was exercised to avoid disturbing the tested area of the samples during the visual and photographic observations, since quite frequently the surface was characterized by loosely attached coating system fragments. The sample pieces were again photographed in full view in color for record. Magnified (about ×3) views of the tested area were also photographed in monochrome. The tested area was microscopically reexamined to make note of any testing-caused changes in surface characteristics. Scrapings were taken from near center of the tested area for X-ray diffraction samples for crystallographic comparisons with pretest scrapings. Finally, the samples were sectioned in the center of the tested area and at a relatively unaffected area near the ends of the coolant tubes. The sections were encapsulated and polished for microscopic examination for structure characteristics and changes. Further, the sections were photomicrographed for record and for use in obtaining individual layer and total coating system scaled thickness measurements. These examinations, evaluations, and comparisons are summarized in a later section of this report.

General Operating Procedures

The facility operating procedures for both types of hot testing which were detailed earlier were similar except, of course, for the testing modes themselves. For reference, the following paragraphs describe the sequence of events in a typical facility operation.

After the coating system sample piece to be tested was installed in position in the test facility, the containment vessel was closed, sealed, and thoroughly purged with nitrogen to remove the enclosed air. Following that, the vessel was pressurized to about 20.7×10^4 newtons/meter^2 absolute (30 psia) with nitrogen. With the nitrogen supply closed, the vessel pressure was monitored for leakage. When no leakage was apparent for 15 minutes, the vessel pressure was reduced to about 1.4×10^4 newtons/meter^2 (2 psia); the coating system was conditioned for a minimum of 15 minutes at that pressure, as previously described.

The cooling water supply to the sample piece and heat-flux meter were each adjusted to 3.15 kilograms/second (6.94 lbm/sec, or 50 gal/min) at 344.7×10^4 newtons/meter^2 absolute (500 psia). The cooling water supplies to the plasma generator and other cooled components were also adjusted to their proper levels. The plasma generator was alined on the heat-flux-meter instrumentation, and the spacing of the generator nozzle exit to the heat-flux meter (and sample piece) was set to 8.89×10^{-2} meter (3.5 in.). The hydrogen weight flow rate through the plasma generator was adjusted to 0.273×10^{-3} kilogram/second (0.0006 lbm/sec), and the generator was started by means of a high-frequency current pulse to establish an arc. Then, with the hydrogen plasma stream impinging on the heat-flux meter, the electrical power to the generator was adjusted to produce the desired heat-flux level. As described in appendix B, the heat flux at the heat-flux meter is indicated by thermocouple readings. When the proper heat-flux level was reached, the coating system sample piece was moved into the plasma stream to replace the heat-flux meter. The planned testing period was then completed with constant electrical power and hydrogen flow rate settings. At the end of the testing period, the heat-flux meter was again moved into the plasma stream to replace the sample piece and verify the heating level, and then the electrical power was reduced to zero. In this position, the coating system could be readily inspected by means of the observation ports in the containment vessel.

RESULTS AND DISCUSSION

The coating systems evaluated in the hydrogen plasma facility can be classified into three general groups. One group contained zirconium oxide (ZrO_2, or zirconia) as the primary thermal insulator. A second group contained aluminum oxide (Al_2O_3, or

alumina) for this purpose, while the third group involved modifications of these or alternate thermal insulators. Initially, one specimen from each system was given a series of 30-second exposures in steps of increasing heat flux of 1.635×10^6 watts/meter^2 (1 Btu/(in.^{2})(sec)) from 1.635×10^6 watts/meter^2 (1 Btu/(in.^{2})(sec)) to 19.6×10^6 watts/meter^2 (12 Btu/(in.^{2})(sec)). Fresh second specimens of promising systems were then given a 19.6×10^6-watts/meter^2 (12-Btu/(in.^{2})(sec)) exposure for a total of 30 minutes. Each specimen was examined visually and by X-ray diffraction before and after testing. Metallographic cross sections of one cold end and of the hot zone were also made and studied for each tested specimen. The results of these examinations are presented in the following sections. The second photomicrographs of the coolant tube end regions will be identified as "untested" or "before testing," while those of the tested area will be identified as "tested" or "after testing."

In considering the test results, it should be noted that the general testing procedure - uniform heat-flux testing for all coating systems - probably gave rise to a different surface temperature for each system. Coating systems with high thermal resistances had higher surface temperatures than systems with lower thermal resistances for the same heat flux. Therefore, some of the differences in surface effects noted in the tested samples may have been influenced by this temperature nonuniformity. Further, because of the relatively low hydrogen plasma weight flow rate, tested coating system surface features may be different from those exposed to the same heat flux for the same time period in an actual nuclear rocket thrust chamber. In an actual chamber, the more loosely attached coating system fragments would probably be blown away, while in the plasma tests they remain. From the standpoint of having most of the coating material present for examination after testing, the plasma tests have a decided advantage over actual chamber tests for materials selection and/or coating screening studies.

Zirconium-Oxide-Based Coatings

Three coating systems (1, 2, and 5) incorporated zirconia as the primary thermal insulator and are described in table I. System 1 incorporated a molybdenum underlayer and a nickel-chromium solid-solution alloy (nichrome) graded with zirconia to metal-free zirconia on the surface. Similarly, system 2 used a molybdenum underlayer and molybdenum graded with zirconia to an outer layer composed of zirconia and hafnium oxide (HfO_2, or hafnia). System 5 consisted of discrete layers of molybdenum, nichrome, and zirconia without grading. When the grading technique is not used in a coating system in this study, that system will be referred to as "layered." Visual, X-ray diffraction, and coating thickness data obtained on these systems, before and after testing, are summarized in table III. It must be noted that, even though reasonable care was

taken in the surface scraping process for the X-ray diffraction tests, material from one or more subsurface layers may have inadvertently been included.

Table III shows that generally all plasma-sprayed zirconia coatings were yellow-white in color with some metal inclusions in the surface (either from the electrode of the plasma spray torch or from residual metal particles in the spray hopper). Figure 7(a) presents a low-magnification photograph of a typical specimen surface in the as-coated condition; in this case, the surface of system 1:B. System 1:B refers to coating system type 1 supplied by contractor B (see table I). This designation method will be used throughout this report.

X-ray diffraction analysis indicated that most of the coatings in this group contained cubic, or "stabilized," zirconia. Pure zirconia at room temperature is monoclinic in crystal form and reversibly transforms to a tetragonal form near 1366 K (2460° R). Accompanying that phase change is a rather abrupt, crack-promoting density increase of about 8 percent. When calcium oxide (CaO, or calcia) or yttrium oxide (Y_2O_3, or yttria) is added to zirconia in solid solution, the zirconia becomes partially or fully stabilized, depending on the relative amount of the additive. Stabilized zirconia is cubic crystalline in form and retains that form to its melting temperature. Stabilized zirconia is characterized by uniform thermal expansion characteristics. The coating vendors were not required to report their methods of zirconia stabilization. Except in a few cases, the metallic surface inclusions were not present in sufficient quantity to be identified by X-ray analysis.

The step test caused some "mud-flat" cracking in all of the zirconia coatings. Those applied by the slurry/cure process (systems 1:E and 5:E) blistered and failed below 8.2×10^6 watts/meter^2 (5 Btu/(in.^{2})(sec)), and were not tested further. Of the remaining coatings, the tested area surfaces, in some cases, showed a golden color attributed to the additional ZrN phase detected by X-ray diffraction. Since the test chamber was normally purged with nitrogen before testing, enough residual nitrogen was apparently present to form this compound. Also, some slight thickness loss due to erosion was generally observed. Figure 7(b) illustrates the typical surface condition in the tested area after step testing to the 19.6×10^6-watt/meter^2 (12 Btu/(in.^{2})(sec)) level (system 1:B is shown here).

After endurance testing, all systems showed more severe surface cracking and erosion. However, all these coatings remained in place and their typical appearance is shown in figure 7(c). No major differences could be seen between the three different systems. All systems also showed some tiny metallic globules on the surface. These globules may have been one of the coating constituents, but there was an insufficient quantity of material to identify by X-ray diffraction. This identification method normally requires the presence of from 1 to 5 percent of a phase.

The same phases (cubic zirconia, underlayer material, etc.) were also detected by X-ray diffraction after the endurance test as they were after step testing. Here,

however, the ZrN phase was detected in almost every case. One test was conducted in which helium was used to purge the test chamber instead of nitrogen (see table III: system 5:D (repeat)). Here, no ZrN was detected by X-ray diffraction. Since this specimen still showed mud-flat cracking, the cracks are probably not due to the presence of ZrN. The latter specimen also showed a very shiny, silver-colored surface. Like the systems which showed the metal globules, insufficient material was present to identify it with X-ray diffraction.

Metallographic cross sections of an untested and a tested area of all tested specimens were used to measure coating loss. It is apparent from an examination of the step-test and endurance-test data presented in table III that the application methods used by the vendors gave rise to nonuniform coating thicknesses. In addition to the significant differences in pretest coating thickness between supposedly identical samples, similar differences in coating thickness were frequently noted at different points on the same sample. All the samples used in this study exhibited a similar lack of thickness uniformity. Based on the measurements, in fact, some coating systems appear to grow thicker with testing, while others decrease in thickness. Section photomicrographs indicate the individual underlayers of metal-ceramic mixtures were most often applied in thicknesses less than requested. In most of these cases, an attempt was apparently made to achieve the desired overall coating system thickness by applying the outer layer in thicknesses much greater than requested.

Typical sections of the zirconia coating as exemplified by system 1:B are shown in figure 8. Each section photomicrograph presented in this and the following sections was taken at the crown of the center tube in the area designated. Figure 8(a) shows the untested and tested area sections after the step test to 19.6×10^6 watts/meter^2 (12 Btu/(in.^{2})(sec)), while figure 8(b) shows similar sections after the endurance test. These photomicrographs indicate the difficulty of obtaining good, uniform grading of metal (white) to oxide (gray) that was experienced by nearly all the vendors. (In fact, this figure is very similar to those of system 5 where the coating was not graded, but layered.) The metal-ceramic underlayers appear to have been deposited thinner than requested and then the total coating thickness in the specification was achieved by depositing a somewhat thicker layer of zirconium oxide. Perhaps the vendors used the metal and oxide percentages listed in table I as the basis for mixing their spray powders - neglecting the differences in deposition efficiency when a metal and an oxide are sprayed simultaneously. In figure 8 and other comparative section photographs made for this study, some differences in appearance of some subsurface coating system layers between the untested and tested conditions are noticeable. The observer might be tempted to identify these differences as changes of constituent content or state due to phase transformation, melting, vaporization, or agglomeration caused by the testing procedure. While any or all of these processes may indeed contribute to the appearance changes, conclusions based on these assumptions might be greatly misleading. Again

here it must be noted that essentially the same differences in sublayer appearance between the untested and tested section locations might have existed even before testing. A rigorous review of the many photomicrographs made for this study indicates that the lack of uniform point-to-point coating application renders most tested-untested sublayer section comparisons inconclusive.

The best grading job was achieved in system 2:A; sections of this system before and after endurance testing are shown in figure 9. Even here, however, the zirconia-hafnia outer layer is slightly thicker than specified (about 0.13×10^{-3} m (0.005 in.) instead of 0.1×10^{-3} m (0.004 in.)) but the general tolerances in plasma spraying are usually $\pm0.0254\times10^{-3}$ meter (0.001 in.). The tested-area photomicrographs of figures 8 and 9 both show a light-colored phase on the surface of the gray oxide layer, along cracks in the oxide, and in some cases within the oxide. When viewed with a microscope, this phase is golden in color. Furthermore, since almost none of this phase was observed in the helium-purged specimen discussed previously, it is believed to be ZrN.

Thus, in all the plasma-sprayed systems, little difference in structural performance could be noted between nichrome grading, molybdenum grading, or metal-oxide layering. All the coatings remained in place but showed considerable mud-flat cracking and some erosion of the most thermally insulating outer oxide layer. Most of the graded systems were not uniformly graded and actually closely approximated layered systems. As a result, this similarity in behavior is not unexpected.

Even system 2 which was somewhat better graded (and had a surface layer which included monoclinic HfO_2) was not much different in its response to the tests employed.

Aluminum-Oxide-Based Coatings

Table I contains the compositions of two systems based on aluminum oxide as the primary thermal insulator: system 3, nichrome-graded alumina with a molybdenum underlayer; and system 4, a molybdenum-nichrome-alumina layered system. Visual, X-ray diffraction, and coating thickness data obtained on these systems, before and after test, are summarized in table IV.

Table IV shows that generally all plasma-sprayed alumina-based coatings were white in appearance with some metal inclusions - either due to residual metal particles in the powder hopper or to tungsten electrode material from the plasma torch. A typical surface view of an as-deposited aluminum oxide coating (system 4:D) is shown in figure 10(a). The slurry/cure coatings 3:E and 4:E were yellow-green with glassy fibers adhering to their surfaces.

According to the X-ray diffraction data, most of the alumina coatings contained more than the alpha alumina (corrundum) phase and underlayer materials. Gamma and eta alumina, unstable phases, were detected, along with a number of intermetallic com-

pounds. The alumina modifications were probably produced by the extremely rapid quenching rates characteristic of the plasma-spray application technique. The foreign compounds probably resulted from trace impurities in the coating materials and/or from gradual sprayer electrode disintegration. The effects on coating system performance of the presence of these other-than-specified phases and materials are unknown, but with development their quantities could probably be reduced. In the slurry/cure coatings, only the alpha-phase alumina was detected, probably because the cold application method favors better material control.

Except for the slurry coatings, which showed partial spalling and cracking, the step test did little to screen the systems studied. While there was some erosion in most thermal sprayed coatings, as illustrated in figure 10(b), this erosion was slight and produced a number of small valleys in the hot zone rather than any gross material loss. In some of the systems, the unstable gamma or eta alumina was no longer detected by X-ray diffraction although others still contained the gamma phase. Both of the slurry/cure systems contained some $MoSi_2$ and a spinel, probably $NiAl_2O_4$. System 3:B contained chromium nitride, which may have formed by a process similar to the ZrN discussed in the preceding section. Table IV shows that some coatings were apparently thicker after testing than before. Because of the previously described nonuniformity of coating application on the samples, however, no meaningful conclusions can be made about the effect of testing on coating thickness changes solely on the basis of measurements from the photomicrographs.

After endurance testing, all specimens remained intact, as exemplified by figure 10(c), but most showed considerable erosion. The slurry/cure coatings survived but showed greater cracking, blistering, and local spalling. X-ray diffraction studies established that fewer systems contained gamma alumina after this test, indicating that this unstable phase was at least partially reverting back to the alpha form. This phase change is accompanied by a density increase of from 3.60×10^3 kilograms/meter^3 (0.130 lbm/in.^{3}) for the gamma phase to 3.96 kilograms/meter^3 (0.143 lbm/in.^{3}) for the alpha phase (ref. 3). Thus, during exposure there is a shrinkage of the coating, which may have a contributory effect on the loss of thickness observed in this coating group. Thickness losses measured on specimen cross sections at the center tube crown ranged from about 30 percent to about 70 percent, based on the coating thickness at the tube end, with the greatest losses occurring in system 4 (the layered system).

These data suggest that while alumina is less prone to thermal cracking than zirconia, it is more subject to loss of thickness. In some cases, the thickness loss was so severe that the nichrome-rich layers were exposed and melted - thus, having reached temperatures around 1616 K (2910° R) (ref. 4).

Typical sections of step-tested and endurance-tested specimens are shown in figures 11(a) and (b), respectively, for the 4:D system. This is an intentionally layered system; but since the graded systems were also substantially layered, it is typical of the

aluminum oxide coating systems studied. The "untested" photomicrographs show that, as in the case of the zirconia coatings, the underlayer thicknesses were less than requested (total thickness, approx. 0.051×10^{-3} m (0.002 in.) instead of 0.13×10^{-3} m (0.005 in.)), while the oxide layer was thicker than required (0.15×10^{-3} m (0.006 in.) instead of 0.076×10^{-3} m (0.003 in.)). Note again that after both the step test and the endurance test, the coating thickness has decreased markedly.

Figure 12 shows a summary of the history of one slurry/cure coating, system 4:E. The specimen surface was blistered after the step testing to 9.8×10^{6} watts/meter^2 (6 Btu/(in.^{2})(sec)), as shown in figure 12(a). Figures 12(b) and (c) show the untested and the tested zones, respectively, after this exposure. While good metal-oxide grading is observed in the interior layers, no continuous metal underlayers (0.051×10^{-3}-m (0.002-in.) Mo, 0.076×10^{-3}-m (0.003-in.) nichrome) can be seen. The coating process may require some oxide material to react with an active (possibly phosphate) bonding agent and may thus not be capable of depositing metal layers. Approximately 70 percent of this coating was lost during exposure.

Thus, while the plasma-sprayed aluminum-oxide-based coating systems showed less cracking than the zirconia-based coating systems, they lost thickness more rapidly. They also showed tendencies to form a number of additional compounds, as well as to undergo the gamma- to alpha-alumina phase transformation with its attendant shrinkage. These systems were also not uniformly graded - a fact which may have contributed, in some way, to their loss of thickness.

Miscellaneous-Based Coatings

Three coating systems did not fall into either of the previous categories: system 6, a tungsten-based coating; system 7, a nichrome-graded alumina coating overlayed with zirconia; and system 8, a chromium-oxide- (Cr_2O_3, or chromia) based coating. Visual observations, X-ray diffraction data, and coating thickness measurements for these three coating systems are summarized in table V. Since these systems are so different, each is discussed individually.

Table V shows that system 6 was gray in color with inclusions of copper visible on its surface. While the system was predominantly tungsten, it did contain stabilized (cubic) zirconia, copper, and a gold-based brazing material, as described in table I. The brazing material is composed (in wt. %) of about 81.5 gold, 16.5 copper, and 2 nickel. The material is a product of Western Gold and Platinum Company, Belmont, California. Step testing caused several transverse cracks to develop across the tube crown, but no other visible damage occurred. No new phases were detected after step testing, and the apparent thickness loss was small. After endurance testing, the center surface was gold, just like the ZrO_2-coated specimens; but X-ray diffraction did not

detect any ZrN. Again, only a small thickness loss was measured. Figure 13(a) shows the surface of the coating after this exposure. Only one crack was apparent on the left side of the center tube at this magnification. Comparing the microstructures in figures 13(b) (untested area) and (c) (tested area) shows that the integrity of the coating has not been significantly affected by the exposure. While an increase in voids can be seen in the tested-area section, the coating is essentially intact, except that no retained copper was observed near the surface of the cross section.

On the basis of low erosion loss and the lack of gross cracking, system 6 performed the best of all tested.

System 7 involved a graded nichrome-alumina coating with an overlayer of zirconia. This system performed very similarly to the zirconia-based systems. After endurance testing, the surface was visibly cracked and several spalled regions were observed, as shown in figure 14(a). ZrN, the golden surface phase, was also observed after test. Figures 14(b) and (c) show the coating cross sections at the untested and tested zones, respectively. The light-gray outer layer is zirconia - the inner alumina is a darker gray. Note that after test, just as with the zirconia-based coatings, an abundance of the light (golden) phase (probably ZrN) was observed in the zirconia layer. The cracks which formed in the zirconia layer, however, do not extend through the aluminum oxide/nichrome layers.

System 7 generally showed about the same cracking as the zirconia systems, but less erosion, so that such a combination may offer some insurance against deep coating cracks as well as against erosion. Better grading and a thinner zirconia outer layer might improve this coating's performance.

Table V indicates that the slurry/cure coating (system 8) had a green blistered surface and contained considerable chromium oxide (Cr_2O_3, or chromia). This system was to have been underlayed with chromium metal and graded with a mixture of nickel, chromium, and chromia. After step testing to only 9.8×10^6 watts/meter^2 (6 Btu/(in.^{2})(sec)), however, melted metal globules were observed on the surface. Chromia, nickel chromite spinel ($NiCr_2O_4$), and a complex phosphide were detected by X-ray diffraction. The latter may have been the result of a phosphate binder used in coating application. Microstructures of this system showed, as in the case of the other slurry/cure coatings, that considerable oxide was contained even in the metal underlayers. Due to the poor performance of this system even at the relatively low heat flux reached, no further testing was conducted.

CONCLUDING REMARKS

During the course of this investigation, several considerations concerning the testing for and use of coating systems in a nuclear rocket application came to attention.

Testing all candidate coating systems at uniform heat-flux levels, as was done in this study, if not entirely satisfactory. For the same imposed heat flux, the coating temperature level can vary significantly between coating systems because of the differences in their thicknesses and thermal conductivities. Some of the differences in structural effects noted in the coating system samples tested in this study may have been influenced by these temperature differences. Analytical determination of the coating temperature, when the heat flux and thickness are known, cannot be done with acceptable certainty because of the lack of reliable coating system thermal conductivity information. Using the uniform heat-flux test method, some systems could, in fact, experience temperatures higher than those levels which would normally be considered for the materials involved. Most desirably, the coating systems should be tested on the basis of a temperature compatible with the components of the system and an imposed heat flux representative of the intended application. The test procedure for this study did not include specifying a coating system temperature, since a satisfactory means for measuring and continuously monitoring the surface temperature was not available.

Gross coating system structural failures (serious spalling, etc.) were not common in this testing program. Therefore, structural failure should not be used as the sole criterion for screening candidate coating systems. Rather, the performance of a coating system should be judged on its ability to reduce heat flux to an acceptable level for a representative time period. As a result, subsequent testing programs should include the capability to measure the thermal resistance of the coating systems as well as to evaluate their structural stability with testing time.

The coating system samples fabricated for this study by commercial suppliers are assumed to reflect current state-of-the-art coating capability. With that in mind, it is then apparent that better process control, better thickness control, better uniformity of grading the oxide and metal components, and a better knowledge of thermal property data of plasma-sprayed coating systems must be achieved prior to considering such coatings for incorporation into critical thrust chamber designs or to provide design margin.

SUMMARY OF RESULTS

A series of eight different thermal-insulating coating systems were tested with hydrogen plasma to determine their suitability for use in nuclear rocket applications. The maximum testing heat flux was 19.6×10^6 watts/meter^2 (12 Btu/(in.^{2})(sec)). Each sample was examined before and after testing by visual and X-ray diffraction techniques. The coating systems were compared and evaluated after testing. The conclusions are summarized as follows:

1. On the basis of coating loss due to erosion, spalling, and cracking, the thick (0.61×10^{-3} m (0.024 in.)) tungsten-rich coating - system 6:C - performed the best of all coatings tested.

2. The aluminum-oxide graded coating with a zirconia overlay - system 7:D - also showed some promise for minimizing the depth of surface cracking and material loss.

3. Under the test conditions employed, the great majority of the coatings tested did not spall or flake off. The zirconia-based coatings cracked extensively but remained in place; the alumina-based systems eroded significantly but did not crack to any great extent.

4. The general performance of the slurry/cure coatings was poorer than that of the plasma-sprayed systems because they displayed gross blistering, cracking, and spalling. The slurry coatings, however, may merit further study for thrust chamber components with configurations not amenable to plasma spraying, especially in low or moderate heat-flux applications.

Lewis Research Center,
National Aeronautics and Space Administration,
Cleveland, Ohio, October 7, 1971,
112-29.

APPENDIX A

HEAT-FLUX-METER FABRICATION

The function of the heat-flux meter in this study is so important that its structure and fabrication merit special attention here. The heat-flux meter must accurately measure a heat flux nearly identical to that which the coating system sample experiences. To do that, its configuration and cooling capacity ideally should be identical to that of the coating system sample piece. Further, the meter should be able to continuously measure the heat flux for a relatively long period of time to allow for reasonable electrical power adjustment and stabilization periods. The most direct approach was employed; that is, to suitably instrument for use as a heat-flux meter a sample piece identical to those used for coating system samples. The instrumentation method selected was to emplace a very-small-diameter thermocouple assembly in the coolant tube wall at the center of the testing, or heated, area. This general instrumentation method has been used with cooled rocket thrust chambers previously, as described in reference 5, but with larger-size components. The additional complexities introduced by the very small thermocouples and thin wall sections in this study, however, required extensive additional development and are detailed in the following paragraphs.

Channel Preparation and Assembly

Figure 1 details the general construction of the heat-flux meter and coating system sample pieces. Briefly, three 0.305×10^{-3}-meter (0.012-in.) thick, type 347 stainless-steel, coolant tube shells spaced with shims of identical material were fitted into a type 304 stainless-steel block of the configuration shown in figure 1. Views of the block before and after the tube shell fitting are shown in figure 15. Tube shells for the heat-flux meters were specially slotted from skirt to crown to a depth of 0.254×10^{-3} meter (0.010 in.) with a rounded 0.254×10^{-3}-meter (0.010-in.) wide grinding wheel. Two slots were provided, one on each side of the tube shell, for redundant instrumentation. Figure 16 shows the two thermocouple positions to be about 1.524×10^{-3} meter (0.060 in.) apart.

Thermocouple Assembly Fitting

The thermocouple assemblies used were commercially obtained, swaged, grounded-end, 0.254×10^{-3}-meter (0.010-in.) diameter Chromel-Alumel units, as illustrated in

figure 17. Prior to fitting, the thermocouple assemblies and the slotted portions of the tube shells were "flashed" with a thin (about 0.00254×10^{-3} m (0.0001 in.)) gold plating to enhance later brazing. The thermocouple assemblies were introduced into the tube shell slots from the back of the heat-flux-meter block through slot-matching 0.41×10^{-3}-meter (0.016-in.) diameter access holes (see fig. 1) located in the bottom of the tube shell receiving grooves. After forming the thermocouple assemblies to tube shell contour and locating the tips at the tube crown, the units were held in place for final braze attachments by a series of prick-punch "upsets" along each side of the slots, as shown in figure 18.

Assembly Brazing

When the instrument fitting was completed, the entire heat-flux-meter assembly was vacuum-furnace brazed. The braze material was a commercial preparation composed of 82 percent gold and 18 percent nickel by weight. Brazing was accomplished at between 1261 and 1266.5 K (2270° and 2280° R) at a pressure of 0.13 to 0.67 newton/meter^2 absolute (vacuum of 1×10^{-3} to 5×10^{-3} torr). This brazing method overcomes the problems of discontinuous braze attachment in very close fits and severe braze erosion common with very thin wall sections. Relative positions of the thermocouple alloy wires within the sheath were determined by radiography techniques. In this way, the wire pair was oriented parallel to the tube shell surface for minimum bending strain and minimum temperature-gradient-caused measurement error (see ref. 5). The thermocouple leads were terminated in the instrument recess in the back of the heat-flux-meter block. With moderate effort, the brazed area over the thermocouple assembly can be finished to the original tube surface level. A section photomicrograph of an installed thermocouple assembly is shown in figure 19. The section view, taken near the sensing junction, clearly shows the wire pair orientation and complete braze contact with the tube slot and instrument sheath.

Heat-Flux-Meter Performance

The characteristics of the Chromel-Alumel thermocouple assembly did not change significantly during heat-flux-meter fabrication. In spite of the bending and forming operations and the braze cycle, the instrument calibration did not vary more than 2 percent (emf for a specific temperature) from the manufacturer's specifications for the delivered units. This was determined by the results of a supporting calibration study conducted at the Lewis Research Center.

The accuracy of the thermocouple readings is affected by two major factors. First, the very presence of the relatively large thermocouple assembly (0.254×10^{-3} m (0.010 in.) diam) in the 0.305×10^{-3}-meter (0.012-in.) thick tube wall indicates an obvious temperature distortion effect. Also, the apparent high thermal conductivity of the gold-based brazing material used raises the question of whether the temperature gradients at the brazed locations are typical of the general case. The complete effects of these conditions are not resolved, but a compensating factor is that the sensing portion of the thermocouple is a solid mass of mostly type 304 stainless steel (see fig. 17), which has a thermal conductivity essentially identical to that of the tube material. The thermocouple junction mass extends from the bottom of the tube slot to the tube outer surface, with only thin films of brazing material at the interfaces. Therefore, the temperature distortion effect is diminished at the sensing junction itself. On this basis, and including the effects of the previously described maximum thermocouple calibration shift, the precision with which the sample heat flux was established for this study is estimated to be within ±10 percent at all values from 0 to 19.6×10^6 watts/meter^2 (12 Btu/(in.^{2})(sec)).

The heat-flux meters have demonstrated excellent reliability. Some of these have operated at a heat flux of 19.6×10^6 watts/meter^2 (12 Btu/(in.^{2})(sec)) or a surface temperature of 1027 K (1850° R) for accumulated times to several hours, including as many as 100 on-off cycles. The presence of the thermocouples in the thin tube shell walls did not significantly weaken the structure, since each heat-flux meter was internally hydraulically pressure-tested to about 1103×10^4 newtons/meter^2 absolute (1600 psia) before use. No failures resulted from this testing procedure.

APPENDIX B

HEAT-FLUX-METER CALCULATIONS

Heat-Flux and Measured-Temperature Relation

From the dimensions shown for the heat-flux-meter tube configuration in figure 1(c), the tube cross-sectional area A and hydraulic diameter D may readily be computed to be 0.040039×10^{-3} meter^2 (0.06206 in.^{2}) and 6.2205×10^{-3} meter (0.2449 in.), respectively. (All symbols are defined in appendix C.) Cooling water was supplied to the heat-flux meter at the rate of 3.16×10^{-4} meter^3/second (50 gal/min) at a pressure of 344.7×10^4 newtons/meter^2 absolute (500 psia). Data from a large number of runs indicated the mean stabilized coolant temperature to be about 305.5 K (550° R) and the coolant temperature rise through the heat-flux meter at testing conditions to be only about 0.55 K (1° R). By using water density values from reference 6, the average water velocity v and the weight flow rate w through the heat-flux meter were determined to be 26.274 meters/second (1034 in./sec) and 3.143 kilograms/second (6.93 lbm/sec), respectively. Reference 7 presents an experimentally based correlation for the wall-to-coolant heat-transfer coefficient for water at subcritical temperatures flowing in smooth tubes in fully developed turbulent flow. The equation is

$$h = 0.019\left(\frac{k_f}{D}\right)\left(\frac{DG}{\mu_f}\right)^{0.8}\left(\frac{C_p\mu}{k}\right)_f^{0.4}$$

where the coolant properties are introduced at a film temperature T_f defined as

$$T_f = 0.5(T_{w,c} + T_c)$$

and the heat-transfer coefficient is defined as

$$h = \frac{q}{T_{w,c} - T_c}$$

Considering the ratio of the distance from the heat-flux-meter tube water inlet to the center of the heated area to the hydraulic diameter of the tubes (see fig. 1(a)), it is apparent that the heated area is in the turbulent-flow entry region. Data summarized in reference 8 indicate that for this estimated length-to-hydraulic-diameter ratio (9.18, assuming the inlet flow length to be 5.72×10^{-2} m (2.25 in.)) and a 90° flow bend in a

round tube, the multiplying correction factor for the coefficient in the correlating equation is about 1.30. Applying this correction, the modified correlating equation may be written

$$h = 0.0247\left(\frac{k_f}{D}\right)\left(\frac{DG}{\mu_f}\right)^{0.8}\left(\frac{C_p\mu}{k_f}\right)^{0.4}$$

By using the modified correlating equation along with the geometry and flow conditions, values of coolant specific heat $C_{p,f}$ from reference 9 and values of viscosity μ_f and thermal conductivity k_f from reference 10, the curve shown in figure 20 was developed. This curve presents the coolant tube internal heat-transfer coefficient h as a function of coolant film temperature T_f.

Because the coolant tubes have a large ratio of diameter to wall thickness, the assumption that the hot-gas-side and coolant-side heat-transfer areas are equal can be made with acceptable accuracy. Consequently, from continuity considerations, and assuming lateral temperature gradients are small, the hot-gas-side and coolant-side heat fluxes are assumed to be equal. With this in mind, then, the equation

$$q = \frac{k_w}{b}(T_{w,g} - T_{w,c}) = h(T_{w,c} - T_c)$$

can be written. Simple manipulation of this expression results in the form

$$T_{w,c} = \frac{\frac{k_w}{b}T_{w,g} + hT_c}{\frac{k_w}{b} + h} \tag{1}$$

Values of the tube wall thermal conductivity k_w can be found in reference 10. Using the coolant tube wall thickness $b = 0.305\times10^{-3}$ meter (0.012 in.), the definition of T_f, the information of figure 20, and the assumption

$$k_w = f\left[0.5(T_{w,g} + T_{w,c})\right]$$

then the multipoint, interative solution of equation (1) results in the curve shown in figure 21. That curve relates the hot-gas-side wall temperature $T_{w,g}$ to the coolant-side wall temperature $T_{w,c}$.

With the information contained in figure 21, the expression

$$q = \frac{k_w}{b} (T_{w,g} - T_{w,c})$$

and the assumption for tube wall thermal conductivity stated earlier, the relation between heat flux q and hot-gas-side wall temperature $T_{w,g}$ can readily be developed. That relation is shown in figure 22.

The calorimeter thermocouple sensing junctions are estimated to be at a depth of about one-half the thermocouple assembly diameter from the hot-gas side of the tube wall. This geometry is indicated in figure 1(c) and appendix A, and the assumption was shown to be valid by a number of cross-section photomicrographs of sample thermocouple installations. Assuming the temperature gradient across the tube wall to be linear, the expression

$$\frac{T_{w,g} - T_m}{d} = \frac{T_m - T_{w,c}}{b - d}$$

can be written, where T_m is the temperature measured by the embedded thermocouple and d is the thermocouple depth, measured from the hot-gas-side wall surface. Solving this for T_m results in

$$T_m = \frac{(b - d)T_{w,g} + (d)T_{w,c}}{b}$$

Note for the configuration used in this study, $d = 0.13 \times 10^{-3}$ meter (0.005 in.). By means of this relation and the information of figures 21 and 22, a curve relating the measured temperature to the heat flux to the calorimeter can be constructed. This curve is shown in figure 23. Then, observing all the stated operating conditions, the relation shown in figure 23 permits the adjusting and monitoring of the heat flux by adjusting (by adjusting electrical power) and monitoring the readout of a single thermocouple on a strip chart. The 344.7×10^4-newton/meter^2-absolute (500-psia) water supply pressure to the calorimeter limits the maximum allowable heat flux (without boiling) to about 30.4×10^6 watts/meter^2 (18.6 Btu/(in.^{2})(sec)) by virtue of its 515 K (927° R) saturation temperature.

APPENDIX C

SYMBOLS

A cross-sectional or surface area, m^2; $in.^2$

b coolant tube wall thickness, m; in.

C_p specific heat at constant pressure, J/(kg)(K); Btu/(lbm)(^oR)

D hydraulic diameter, 4A/wetted perimeter, m; in.

d thermocouple junction depth, m; in.

G weight-flow flux, w/A, kg/(sec)(m^2); lbm/(sec)($in.^2$)

h heat-transfer coefficient, W/(m^2)(K); Btu/($in.^2$)(sec)(^oR)

k thermal conductivity, W/(m)(K); Btu/(in.)(sec)(^oR)

q heat flux, W/m^2; Btu/($in.^2$)(sec)

T temperature, K, ^oR

v velocity, m/sec; in./sec

w weight-flow rate, kg/sec; lbm/sec

μ viscosity, N-sec/m^2; lbm/(sec)(in.)

Subscripts:

c coolant stream static or coolant side

f coolant film or coolant film temperature

g gas or hot-gas side

m measured

w wall

REFERENCES

1. Robbins, William H.; Bachkin, Daniel; and Medeiros, Arthur A.: An Analysis of Nuclear-Rocket Nozzle Cooling. NASA TN D-482, 1960.

2. Hjelm, Lawrence N.; and Bornhorst, Bernard R.: Development of Improved Ceramic Coatings to Increase the Life of XLR99 Thrust Chamber. Research-Airplane-Committee Report on Conference on the Progress of the X-15 Project. NASA TM X-57072, 1961, pp. 227-253.

3. Ault, Neil N.: Characteristics of Refractory Oxide Coatings Produced by Flame-Spraying. J. Am. Ceram. Soc., vol. 40, no. 3, Mar. 1, 1957, pp. 69-74.

4. Hansen, Max: Constitution of Binary Alloys. Second ed., McGraw-Hill Book Co., Inc., 1958.

5. Curren, Arthur N.; Price, Harold G., Jr.; Krueger, Roger C.; and Manning, Frank L. C.: Experimental Heat-Transfer Study of a Regeneratively-Cooled Hydrogen-Fluorine Rocket Engine at Low Chamber Pressures. NASA TN D-4178, 1967.

6. Keenan, Joseph H.; and Keyes, Frederick G.: Thermodynamic Properties of Steam. John Wiley & Sons, Inc., 1966.

7. Swenson, H. S.; Kakarala, C. R.; and Carver, J. R.: Heat Transfer to Supercritical Water in Smooth-Bore Tubes. Paper 64-WA/HT-25, ASME, Nov. 1964.

8. Kays, W. M.: Convective Heat and Mass Transfer. McGraw-Hill Book Co., Inc., 1966.

9. Eckert, E. R. G.; and Drake, Robert M., Jr.: Heat and Mass Transfer. Second ed., McGraw-Hill Book Co., Inc., 1959.

10. Tebo, F. J.: Selected Values of the Physical Properties of Various Materials. Rep. ANL-5914, Argonne National Lab., Sept. 1958.

TABLE I. - SUMMARY OF SPECIFICATIONS AND SOURCES OF COATING SYSTEMS EVALUATED

[Coating systems all on 0.3048-mm (0.012-in.) type 347 stainless steel.]

Type	Design specifications				Contractor-reported thickness (average)							Other contractors[b]
	Layer	Material,[a] percent by weight	Thickness		Sample piece						By contractor[b]	
			mm	in.	I		II		III			
					mm	in.	mm	in.	mm	in.		
1	1	Mo	0.0508	0.002	0.0457	0.0018	0.0737	0.0029	0.0584	0.0023		B
	2	70 Nichrome-30ZrO_2	.0508	.002	.0584	.0023	0.686	.0027	.0584	.0023		E
	3	30 Nichrome-70ZrO_2	.0508	.002	.0533	.0021	.0559	.0022	.0711	.0028	A	
	4	10 Nichrome-90ZrO_2	.0508	.002	.0533	.0021	.0635	.0025	.0533	.0021		
	5	ZrO_2	.1016	.004	.1067	.0042	.1041	.0041	.1143	.0045		
		Total	0.3048	0.012	0.3174	0.0125	0.3658	0.0144	0.3555	0.0140		
		Total			0.2794	0.0110	0.2921	0.0115	0.2794	0.0110	D	
2	1	Mo	0.0508	0.002	0.0610	0.0024	0.0635	0.0025	0.0584	0.0023		
	2	82.58Mo-17.42ZrO_2	.0508	.002	.0508	.0020	.0533	.0021	.0635	.0025		
	3	61.25Mo-38.75ZrO_2	.0508	.002	.0584	.0023	.0584	.0023	.0610	.0024	A	
	4	34.51Mo-65.49ZrO_2	.0508	.002	.0533	.0021	.0533	.0021	.0610	.0024		
	5	63.23HfO_2-36.77ZrO_2	.1016	.004	.1041	.0041	.1118	.0044	.0991	.0039		
		Total	0.3048	0.012	0.3276	0.0129	0.3403	0.0134	0.3430	0.0135		
3	1	Mo	0.0508	0.002								B
	2	70 Nichrome-30Al_2O_3	.0508	.002								E
	3	30 Nichrome-70Al_2O_3	.0508	.002								
	4	10 Nichrome-90Al_2O_3	.0508	.002								
	5	Al_2O_3	.1016	.004								
		Total	0.3048	0.012	0.2921	0.0115	0.3810	0.0150	0.3683	0.0145	D	
4	1	Mo	0.0508	0.002								B
	2	Nichrome	.0762	.003								E
	3	Al_2O_3	.1016	.004								
		Total	0.2286	0.009	0.2743	0.0108	0.2362	0.0093	0.2540	0.0100	D	
5	1	Mo	0.0508	0.002								B
	2	Nichrome	.0762	.003								E
	3	ZrO_2	.1016	.004								
		Total	0.2286	0.009	0.2286	0.0090	0.3048	0.0120	0.2235	0.0088	D	
6	1	95W-5 Nicoro 80	0.1016	0.004								C
	2	85W-12ZrO_2-3Cr	.5080	.020								
		Total	0.6096	0.024								
7	1	Nichrome	0.0508	0.002								
	2	50 Nichrome-50Al_2O_3	.0762	.003								
	3	20 Nichrome-80Al_2O_3	.0762	.003								
	4	ZrO_2	.1016	.004								
		Total	0.3048	0.012	0.2794	0.0110	0.2921	0.0115	0.2997	0.0118	D	
8	1	Cr	0.0508	0.002							E	
	2	56Ni-14Cr-30Cr_2O_3	.0508	.002								
	3	24Ni-6Cr-70Cr_2O_3	.0508	.002								
	4	8Ni-2Cr-90Cr_2O_3	.0508	.002								
	5	Cr_2O_3	.1016	.004								
		Total	0.3048	0.012								

[a]The ZrO_2 in coating system type 1 by contractor A and the ZrO_2 and HfO_2 in coating system type 2 are described by the contractor as "stabilized."

[b]Coating systems applied by contractors A, B, C, and D were plasma sprayed, while those applied by contractor E were slurry coated and cured.

TABLE II. - SUMMARY OF EXPERIMENTAL PROCEDURES FOLLOWED IN COATING SYSTEM SAMPLE STUDY

Phase	Step
Sample pretest examinations	1. Record photographs taken: a. Full view (color) b. Magnified (×3) of surface (monochrome) 2. Examine surface microscopically for detail. 3. Take coating scrapings from tube ends for post-test X-ray diffraction comparisons.
Sample cold-shock conditioning	1. Cool sample rapidly with liquid nitrogen (in tubes) from ambient temperature. 2. Allow sample to return to ambient temperature. 3. Reexamine surface microscopically for changes.
Sample hot testing	1. Low-pressure conditioning (15 min at 1.4×10^4 N/m^2 abs (2 psia). 2. Step testing (30 sec each at 1.6, 3.3, . . ., 18.0, 19.6 MW/m^2; 1, 2, . . ., 11, 12 $Btu/(in.^2)(sec)$) 3. Endurance testing (30 min (noncontinuous) at 19.6 MW/m^2; 12 $Btu/(in.^2)(sec)$).
Sample post-test examinations	1. Record photographs taken: a. Full view (color) b. Magnified (×3) of surface (monochrome) 2. Reexamine surface microscopically for changes. 3. Take coating scrapings from tested area for X-ray diffraction comparisons. 4. Make sections at tube ends and heated area and photomicrograph (used for coating thickness measurements and structural change studies).

TABLE III. - EFFECT OF H_2 PLASMA EXPOSURE ON THREE GROUPS OF ZrO_2-BASED COATINGS

[Visual observations; X-ray diffraction data; metallographically measured coating thickness data.]

Coating system: vendor	As received		After step testing				After endurance testing			
	Visual appearance	Surface X-ray diffraction indications	Tested-area visual appearance	Surface X-ray diffraction indications	Approximate coating thickness, mm (in.)		Tested-area visual appearance	Surface X-ray diffraction indications	Approximate coating thickness, mm (in.)	
					Tube end	Tested area			Tube end	Tested area
1:A	Yellow with few metallic particle inclusions	Cubic ZrO_2	Mud-flat cracks on one tube; hairline cracks across gray-yellow tube crowns	Cubic ZrO_2; ZrN; nichrome	0.57 (0.022)	0.31 (0.012)	No cracks; gold color all over hot zone	Cubic ZrO_2; ZrN; nichrome	0.20 (0.008)	0.11 (0.004)
1:B	Smooth, creamy yellow with ~20 percent metal inclusions	Cubic ZrO_2 (W and nichrome - very weak)	Mud-flat cracks on grey tube crowns; some melted Cu on one tube (1:B)	Cubic ZrO_2; ZrN	0.21 (0.008)	0.18 (0.007)	Gold-colored hot zone with gross mud-flat cracking; gray and brown border areas	Cubic ZrO_2; ZrN	0.20 (0.008)	0.15 (0.006)
1:D	Yellow-white and fine-grained with few metal inclusions	Cubic ZrO_2	Gray hot zone with large mud-flat cracks on tube crowns	Cubic ZrO_2; nichrome; Mo (weak)	0.24 (0.009)	0.24 (0.009)	Gold-colored hot zone with gross mud-flat cracking; brown and gray border areas; a few metal islands on surface	Cubic ZrO_2; ZrN; nichrome	0.25 (0.010)	0.20 (0.008)
1:E	Yellow-brown with matte surface and a few green crystals	Monoclinic ZrO_2	Black-gray hot zone showed gross blistering and cracking, failed at 3.3 MN/m^2 (2 $Btu/(in.^2)(sec)$)	Monoclinic ZrO_2; cubic ZrO_2 (?); ZrN	0.43 (0.017)	0.15 (0.006)	Not tested			
2:A	Yellow-gray with metallic inclusions and some brown oxide lumps	Monoclinic HfO_2; cubic ZrO_2	Yellow-white surface oxides; gray discoloration; no visible cracks	Monoclinic HfO_2; cubic ZrO_2	0.47 (0.018)	0.38 (0.015)	Gold-colored, mud-flat-cracked surface with occasional melted, silver-colored droplets	Cubic ZrO_2; ZrN; monoclinic HfO_2 (weak)	0.40 (0.016)	0.31 (0.012)
5:B	Yellow, smooth surface with occasional metallic inclusions	Cubic ZrO_2	Cream-colored hot zone with large mud-flat cracks; gray-brown border areas	Cubic ZrO_2; ZrN	0.20 (0.008)	0.19 (0.007)	Gold, mud-flat-cracked hot zone; gray-brown areas	Cubic ZrO_2; ZrN	0.24 (0.009)	0.20 (0.008)
5:D	Light-yellow surface with very fine particle size of oxide	Cubic ZrO_2	Gold-colored surface with some mud-flat cracking on center tube only	Cubic ZrO_2	0.18 (0.007)	0.14 (0.006)	Gold, grossly mud-flat-cracked surface; gray-brown border areas	Cubic ZrO_2	0.24 (0.009)	0.16 (0.006)
5:D Repeat without N_2 punge of test chamber							Silver-gray shiny surface in hot zone; gross mud-flat cracking; several areas where coating spalled	Cubic ZrO_2; Cr; Mo (weaker)	0.20 (0.008)	0.14 (0.005)
5:E	Yellow-green-brown mud-like surface with green threads in it	Monoclinic ZrO_2	Gray surface with fine deep mud-flat cracks; some spalling and blistering at fringes; "failed" at 8.2 MW/m^2 (5 $Btu/(in.^2)(sec)$) but test completed	Monoclinic ZrO_2; ZrN; cubic ZrO_2 (weaker)	0.25 (0.010)	0.23 (0.009)	Not tested			

TABLE IV. - EFFECT OF H_2 PLASMA EXPOSURE ON TWO GROUPS OF Al_2O_3-BASED COATINGS

[Visual observations, X-ray diffraction data, metallographically measured coating thickness data.]

Coating system: vendor	As received		After step testing				After endurance testing			
	Visual appearance	Surface X-ray diffraction indications	Tested-area visual appearance	Surface X-ray diffraction indications	Approximate coating thickness, mm (in.)		Tested-area visual appearance	Surface X-ray diffraction indications	Approximate coating thickness, mm (in.)	
					Tube end	Tested area			Tube end	Tested area
3:B	White with a few metal inclusions	α-Al_2O_3; γ-Al_2O_3; Mo $AlCr_2$ (weak)	Very little damage	α-Al_2O_3; γ-Al_2O_3; CrN; β-CrN; Mo	0.19 (0.008)	0.25 (0.010)	Gray-white with surface depressions or valleys; some peeling of coating in cold zone	α-Al_2O_3; $NiCr_2O_4$; nichrome; Al_3Mo (?)	0.28 (0.011)	0.18 (0.007)
3:D	Fine-grained, white, smooth surface	γ-Al_2O_3; α-Al_2O_3 (weaker) η-Al_2O_3 (?)	Erosion of Al_2O_3 surface layer and small globules of melted metal	α-Al_2O_3; nichrome	0.43 (0.017)	0.12 (0.005)	White with surface depressions or valleys; looks better than step-heated specimen	γ-Al_2O_3; nichrome; α-Al_2O_3 and Mo_3Al (weaker)	0.29 (0.011)	0.16 (0.006)
3:E	Green and white threads in a mottled green-yellow-tan coating	α-Al_2O_3	Random spalling in a black-and-white matrix; cracks random; rough surface	α-Al_2O_3; spinel ($NiAl_2O_4$?) and $MoSi_2$ (very weak)	0.42 (0.017)	0.38 (0.015)	Gray cellular with mud-flat cracks; local spall to bare metal; silver drops of metal	α-Al_2O_3; Mo (weaker); spinel and ($NiAl_2O_4$?) Ni (very weak)	0.44 (0.017)	0.25 (0.010)
4:B	White sprayed surface with a few metal flakes	α-Al_2O_3; γ-Al_2O_3; nichrome	Gray and white with small valleys	α-Al_2O_3; γ-Al_2O_3	0.16 (0.006)	0.14 (0.005)	White and gray with molten zone on center tube	α-Al_2O_3; Mo_3Al (weaker) Ni (very weak)	0.13 (0.005)	0.06 (0.002)
4:D	Fine-grained white with few metal flecks	α-Al_2O_3; Ni_3Mo; NiMoCr	Islands of Al_2O_3 in metal matrix; some erosion	γ-Al_2O_3; α-Al_2O_3 (weaker) Mo (very weak)	0.20 (0.008)	0.16 (0.006)	Small surface valleys; a few cracks; some metal globules indicating NiCr melted	α-Al_2O_3; nichrome; Mo	0.22 (0.009)	0.12 (0.005)
4:E	Yellow-green surface with glassy white fibers and glassy surface under fiber; cracking where fiber contacts coating	α-Al_2O_3 with unknown element in solid solution	Cracks in white and black areas; randomly located spalling	α-Al_2O_3; spinel ($NiAl_2O_4$?); $MoSi_2$	0.24 (0.010)	0.25 (0.010)	Blistering and local metal melting on black surface; cracks in cooler areas	α-Al_2O_3; nichrome; Mo (weaker); spinel ($NiAl_2O_4$?, very weak)	0.30 (0.012)	0 to 0.10 (0 to 0.004)

TABLE V. - EFFECT OF H_2 PLASMA EXPOSURE ON THREE MISCELLANEOUS COATINGS

[Visual observations, X-ray diffraction data, metallographically measured coating thickness data.]

Coating system: vendor	As received		After step testing				After endurance testing			
	Visual appearance	Surface X-ray diffraction indications	Tested-area visual appearance	Surface X-ray diffraction indications	Approximate coating thickness, mm (in.)		Tested-area visual appearance	Surface X-ray diffraction indications	Approximate coating thickness, mm (in.)	
					Tube end	Tested area			Tube end	Tested area
5:C	Gray metallic with copper-colored inclusions	Cubic ZrO_2; W; Cu; NiCr	Several transverse cracks across tube crowns; no other visible damage	Cubic ZrO_2; W; Cu; NiCr	0.62 (0.024)	0.56 (0.022)	One visible cracks; center gold; no significant erosion	W; cubic Z ZrO_2; Cu; NiCr	0.49 (0.019)	0.44 (0.017)
7:D	Very smooth cream-yellow with a very few globules	Cubic ZrO_2	Yellow-gold with no cracks but some possible erosion	Cubic ZrO_2; ZrN	0.28 (0.011)	0.22 (0.009)	Gross cracking and spalling on center tube; mud-flat cracking in gold surface; not much erosion	ZrO_2; ZrN	0.25 (0.010)	0.23 (0.009)
8:E	Green; blisters; multilayered appearance	Cr_2O_3; nichrome (weaker)	Green to gray color with many melted metal globules; no cracks; stopped at 9.8 MN/m^2 (6 Btu/(in.^{2})(sec))	Cr_2O_3; $NiCr_2O_4$; $(Cr, Ni)_3P$	0.32 (0.013)	0.22 (0.009)	Not tested			

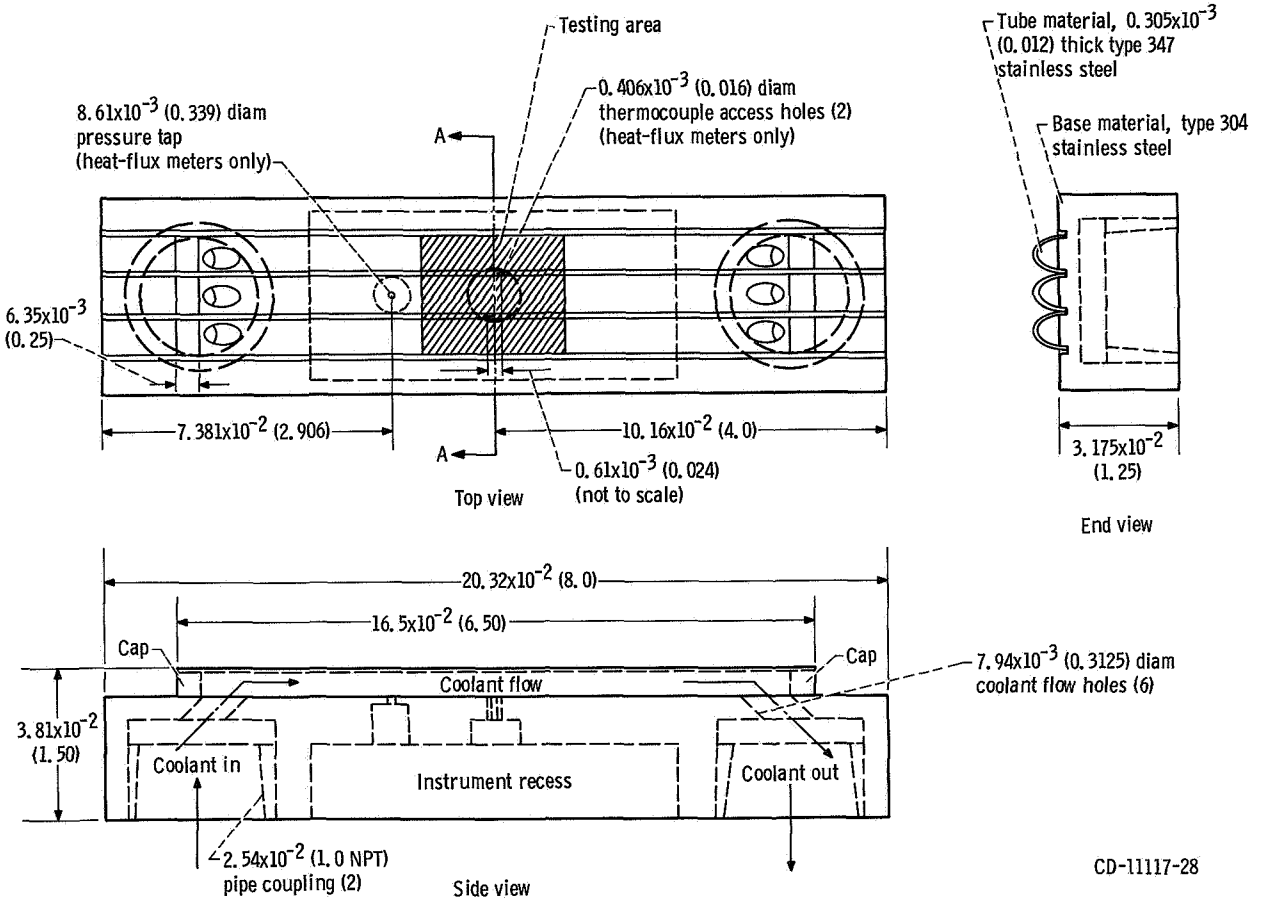

(a) General construction details.

Figure 1. - Coating system sample piece and heat-flux-meter configuration.
(Dimensions are in meters (in.).)

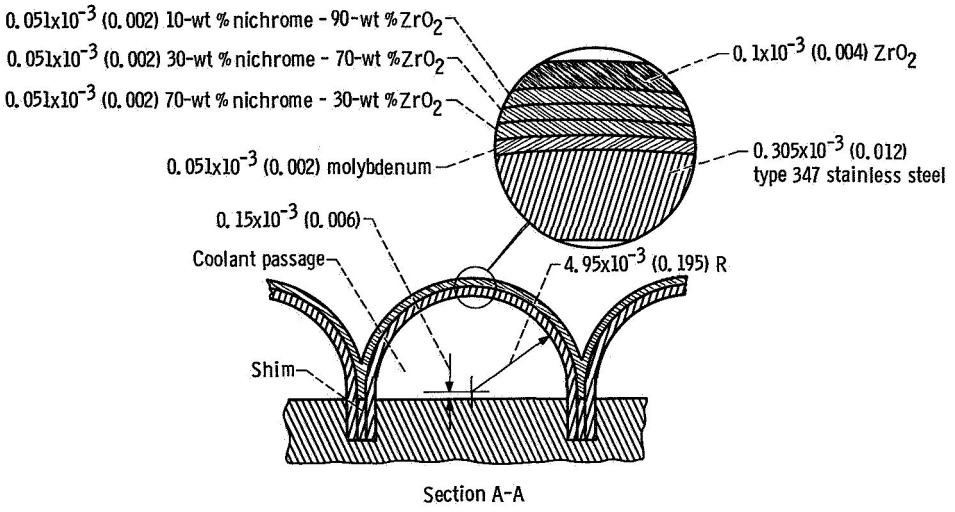

(b) Section view of sample piece with coating system (type 1) applied.

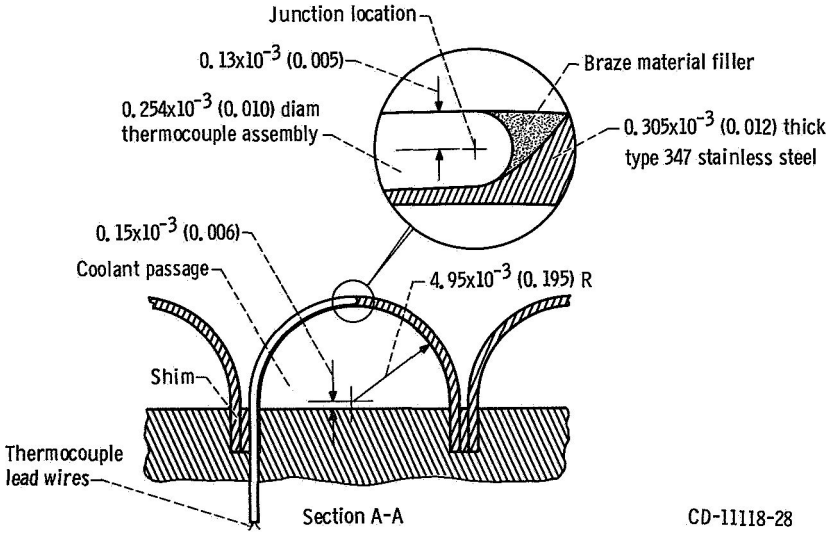

(c) Section view of heat-flux-meter version of sample piece.

Figure 1. - Concluded.

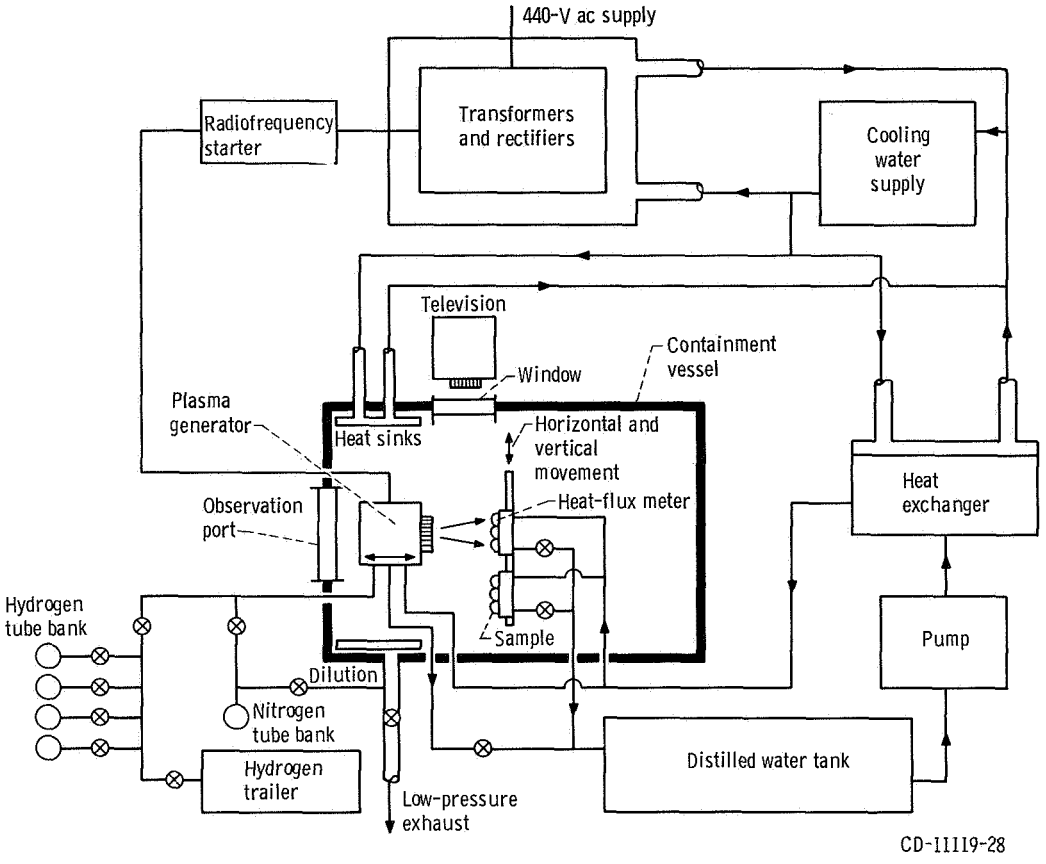

Figure 2. - Schematic of plasma generator test facility.

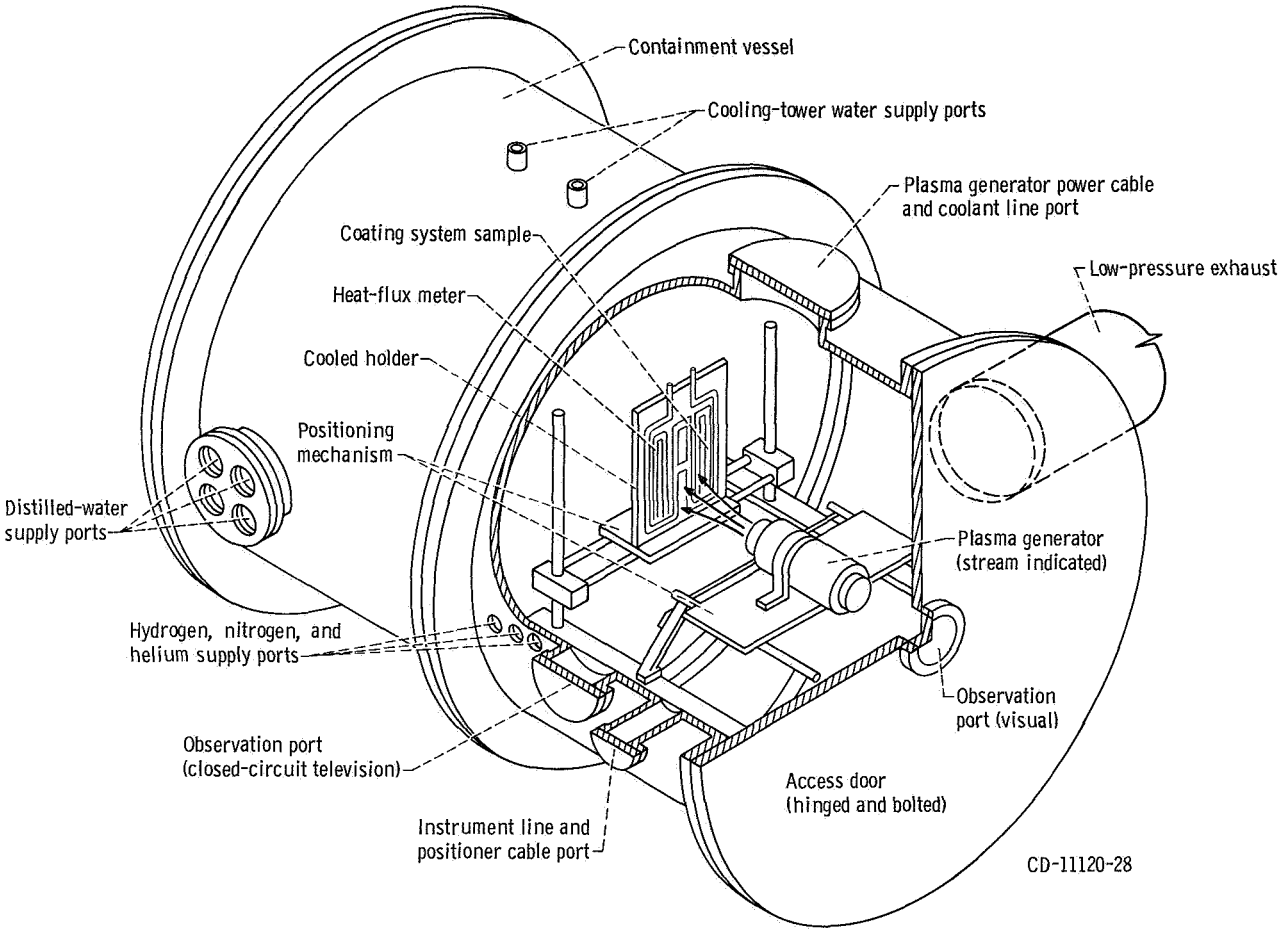

Figure 3. - Cutaway view of containment vessel, showing orientation of plasma generator, sample piece, and heat-flux meter. Tubes, cables, and hoses have been omitted here for clarity.

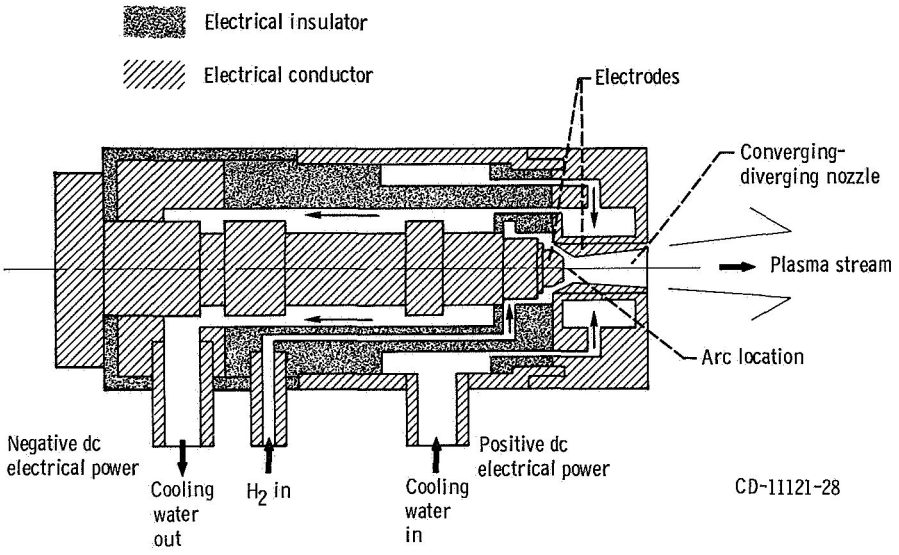

Figure 4. - Schematic of plasma generator used for heating coating system samples in this study. No scale intended.

Layer	Coating system specifications for coated heat-flux meter		
	Material	Thickness	
		mm	in.
1	Molybdenum	0.089	0.0035
2	82.58-wt % Mo - 17.42-wt % ZrO_2	.064	.0025
3	61.25-wt % Mo - 38.75-wt % ZrO_2	.089	.0035
4	34.51-wt % Mo - 65.49-wt % ZrO_2	.064	.0025
5	63.23-wt % HfO_2 - 36.77-wt % ZrO_2	.076	.0030
	Total	0.382	0.0150

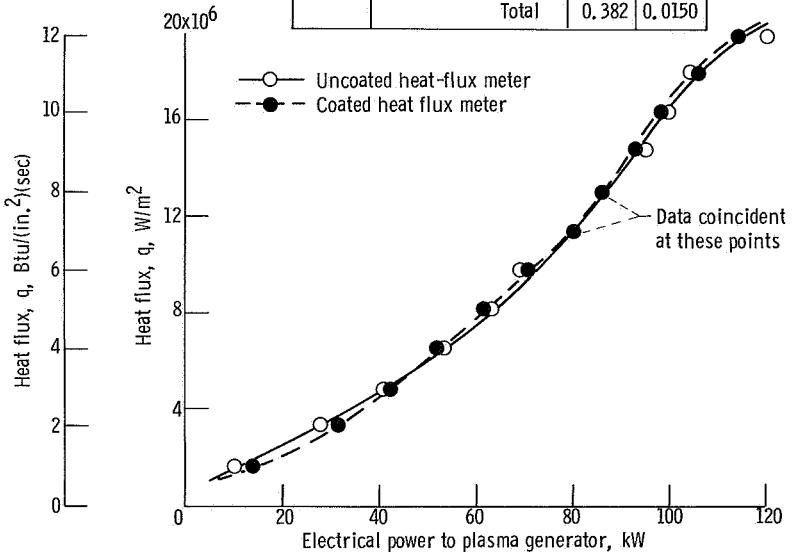

Figure 5. - Comparison of plasma generator electrical power levels for a range of heat-flux levels for an uncoated heat-flux meter and a heat-flux meter protected by a coating system representative of those investigated in this study. Hydrogen gas flow rate for both meters, 0.273×10^{-3} kilogram/second (0.0006 lbm/sec); spacing for both meters, 8.89×10^{-2} meter (3.5 in.).

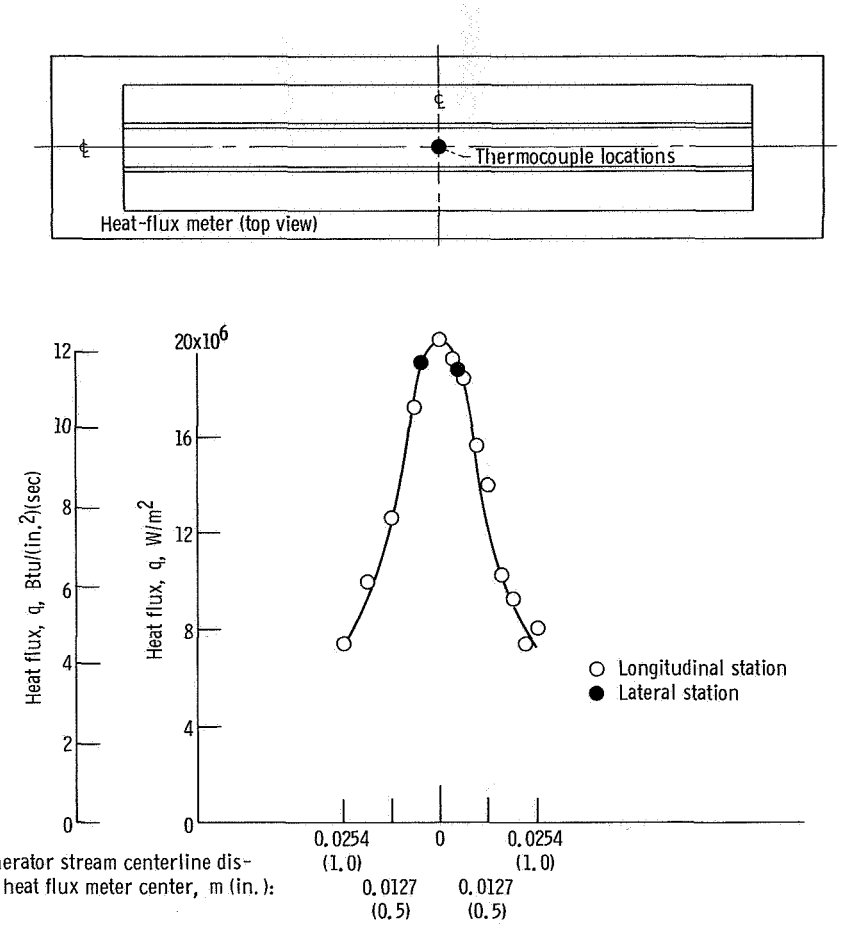

Figure 6. - Heat-flux profile near central position of heat-flux-meter center tube for nominal maximum heat flux of 19.6x10^6 watts/meter^2 (12 Btu/(in.^{2})(sec)). Hydrogen gas flow rate, 0.273x10^{-3} kilogram/second (0.0006 lbm/sec); spacing, 8.89x10^{-2} meter (3.5 in.).

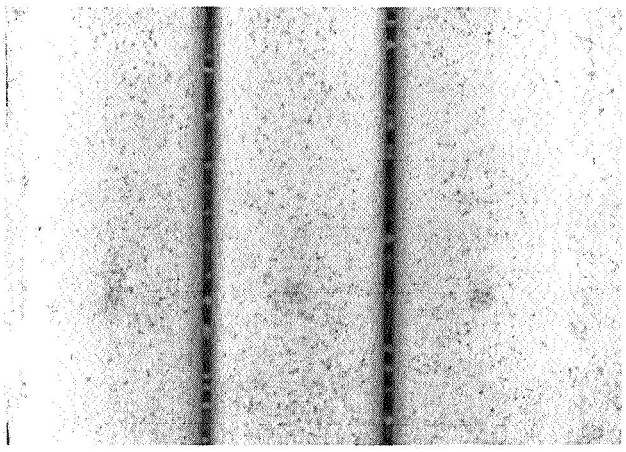

(a) Face view of untested coating system sample.

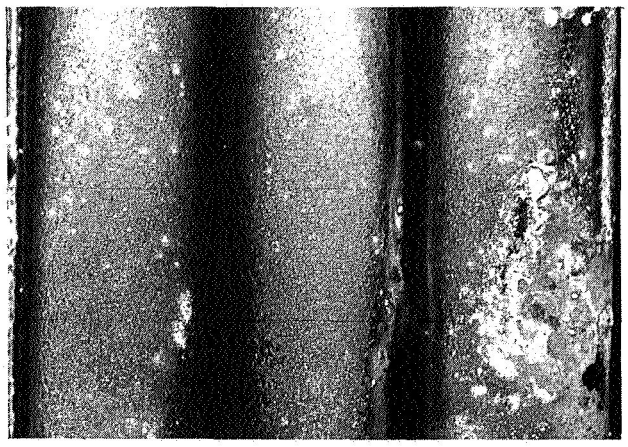

(b) Face view of coating system sample after step testing to 19.6×10^6 watts/meter^2 (12 Btu/(in.^{2})(sec)).

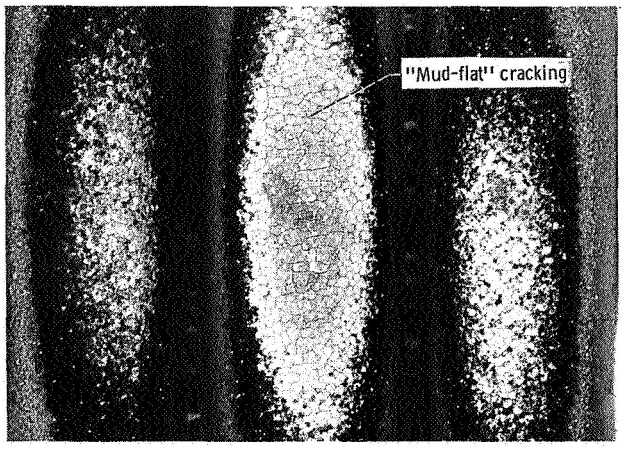

(c) Face view of coating system sample after endurance testing for 30 minutes at 19.6×10^6 watts/meter^2 (12 Btu/(in.^{2})(sec)).

Figure 7. - Coating system surface changes of sample 1:B (Mo sublayer/nichrome-ZrO_2 grading/ZrO_2 outer layer) resulting from hydrogen plasma testing. Original photograph, X3.

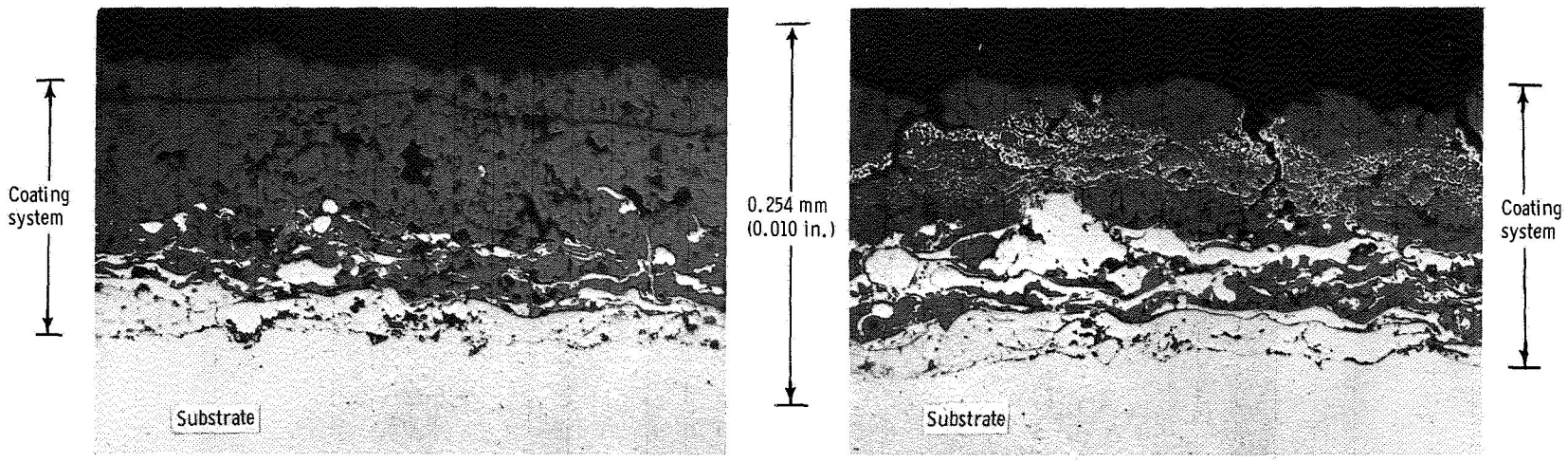

(a-1) Untested. (a-2) Tested.

(a) Section views of coating system before and after step testing to 19.6×10^6 watts/meter^2 (12 Btu/(in.^{2})(sec)).

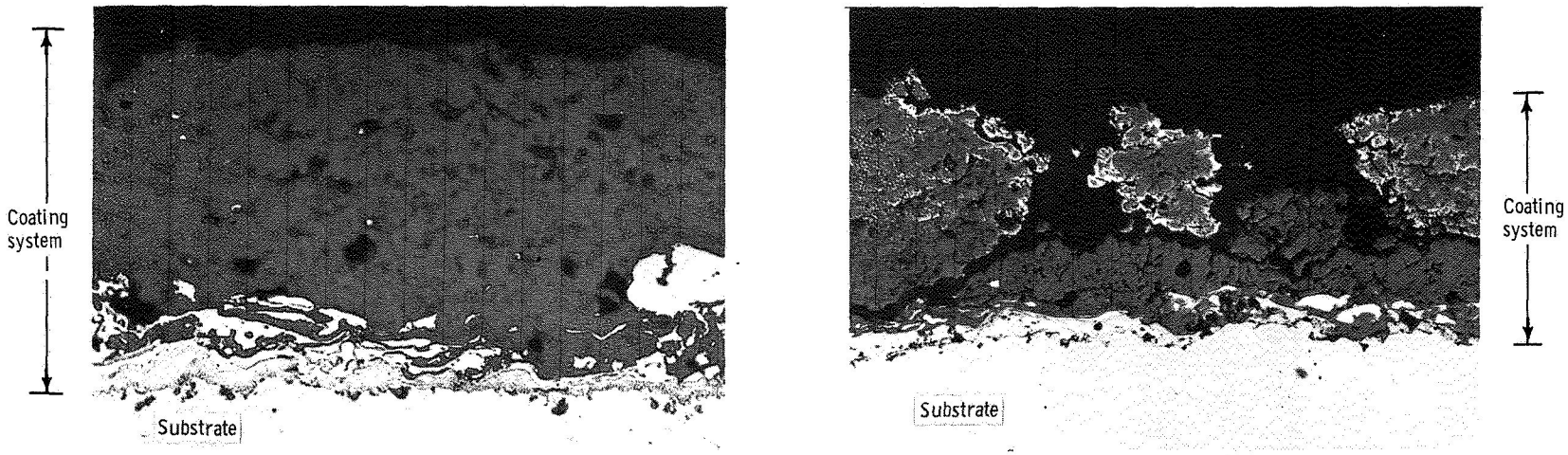

(b-1) Untested. (b-2) Tested.

(b) Section views of coating system before and after endurance testing for 30 minutes at 19.6×10^6 watts/meter^2 (12 Btu/(in.^{2})(sec)).

Figure 8. - Coating system structure changes of sample 1:B (Mo sublayer/nichrome-ZrO_2 grading/ZrO_2 outer layer) resulting from hydrogen plasma testing. Original photomicrograph, X250.

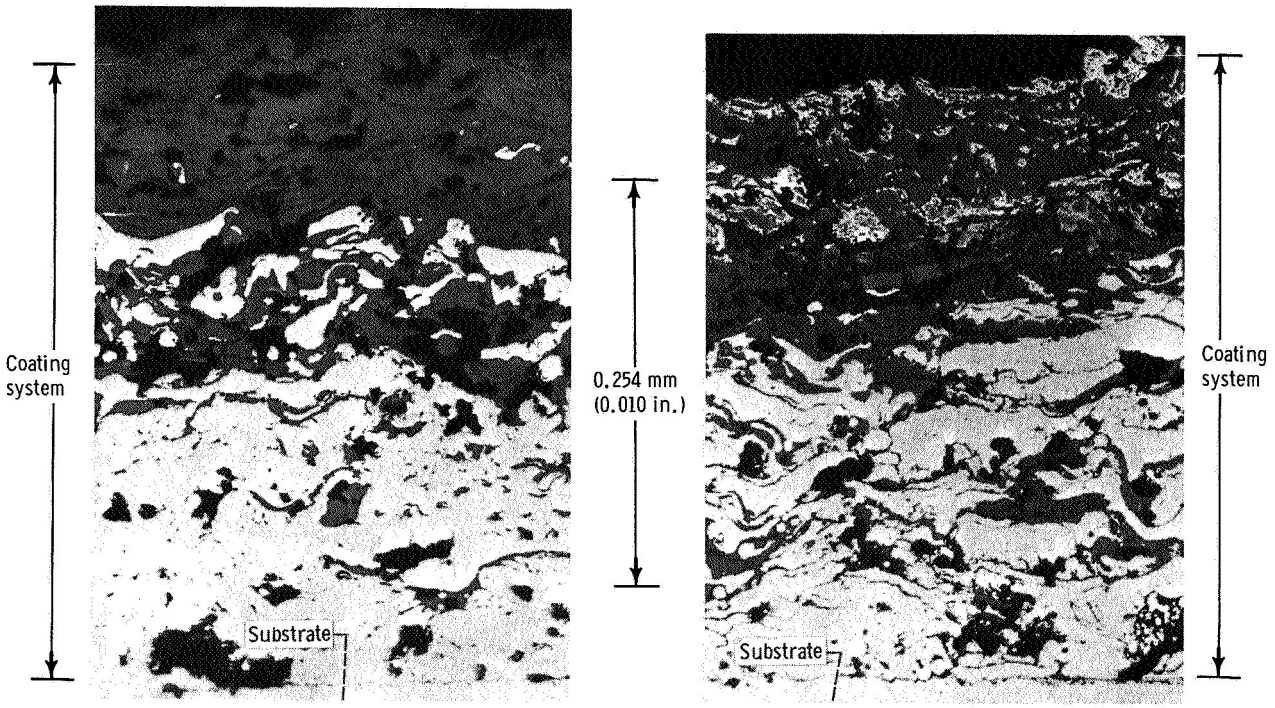

(a) Untested. (b) Tested.

Figure 9. - Section views of best graded coating system structure changes resulting from hydrogen plasma endurance testing for 30 minutes at 19.6×10^6 watts/meter^2 (12 Btu/(in.^{2})(sec)). Coating system 2:A (Mo sublayer/Mo-ZrO_2 grading/HfO_2-ZrO_2 outer layer). Original photomicrograph, X250.

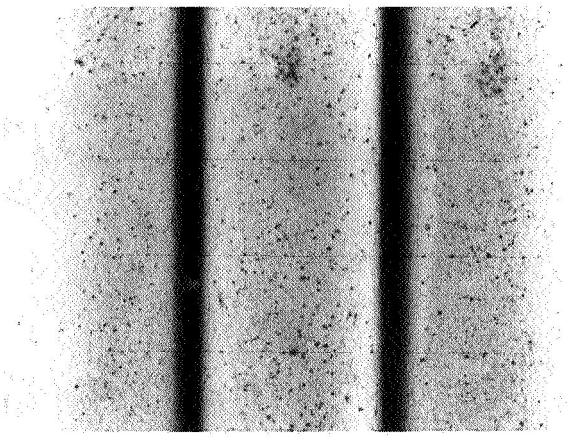

(a) Face view of untested coating system sample.

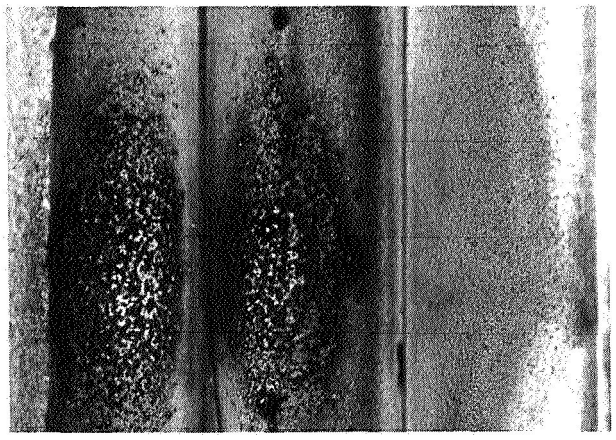

(b) Face view of coating system sample after step testing to 19.6×10^6 watts/meter^2 (12 Btu/in.^{2})(sec)).

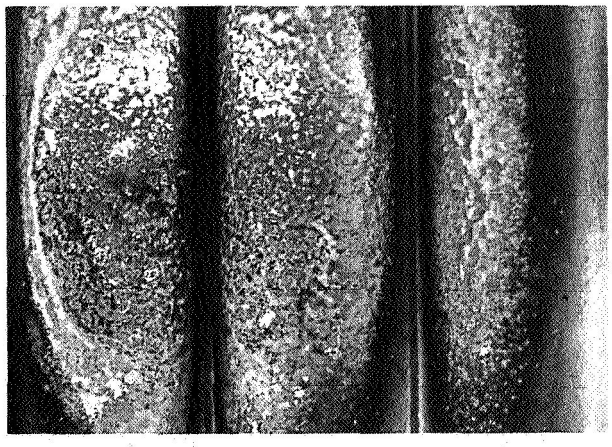

(c) Face view of coating system sample after endurance testing for 30 minutes at 19.6×10^6 watts/meter^2 (12 Btu/(in.^{2})(sec)).

Figure 10. - Coating system surface changes of sample 4:D (Mo sublayer/nichrome middle layer/Al_2O_3 outer layer) resulting from hydrogen plasma testing. Original photograph, X3.

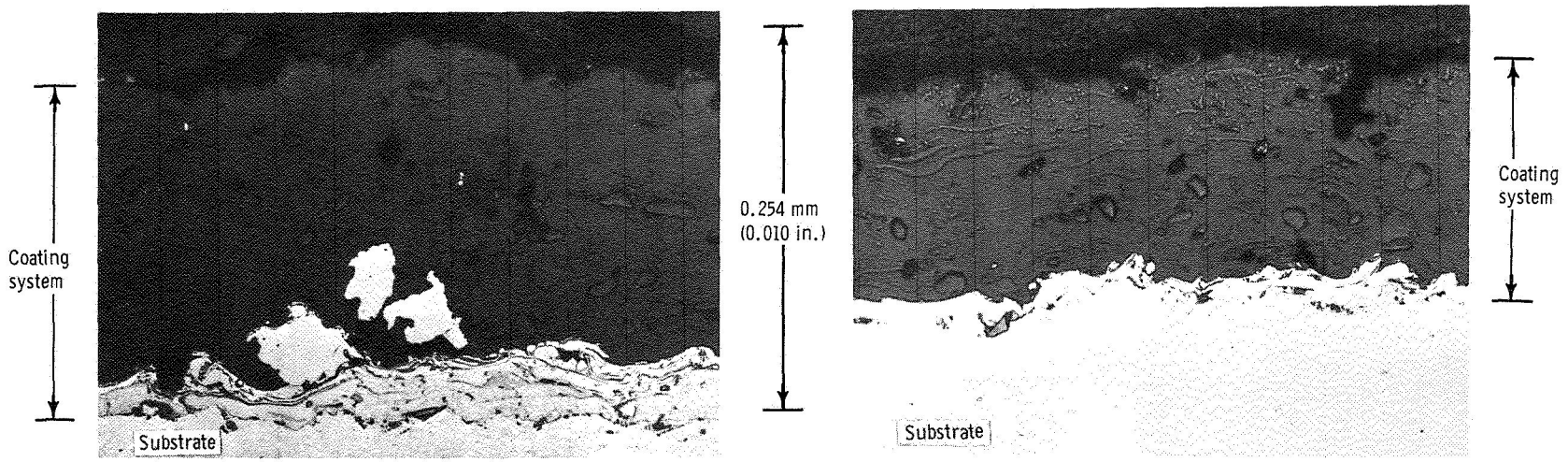

(a-1) Untested. (a-2) Tested.

(a) Section views of coating system before and after step testing to 19.6×10^6 watts/meter^2 (12 Btu/(in.^{2})(sec)).

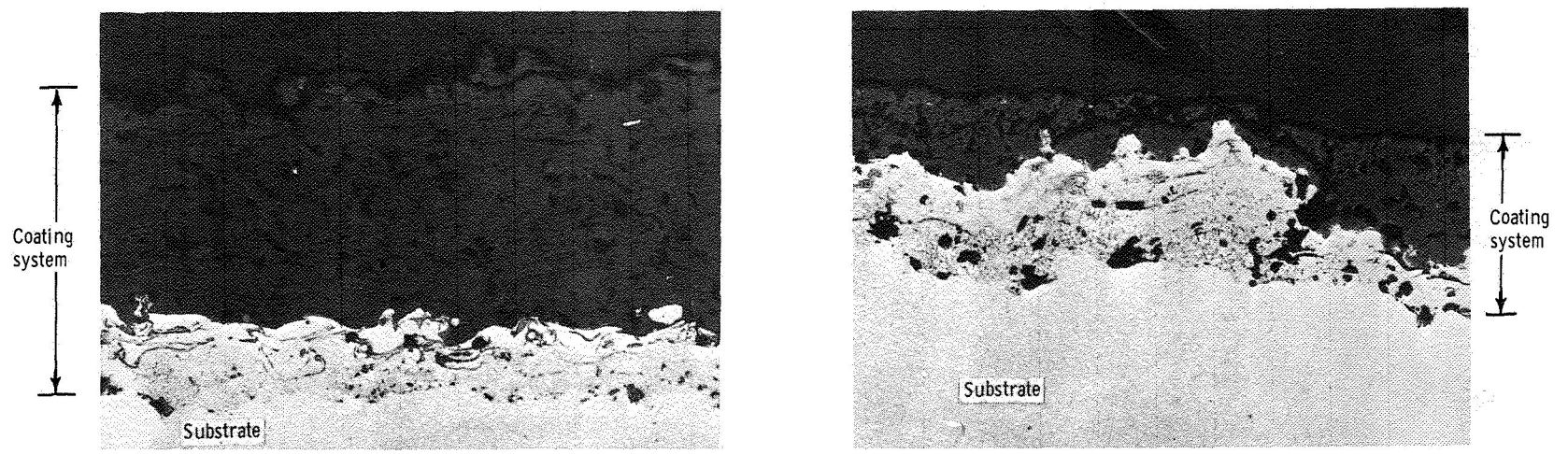

(b-1) Untested. (b-2) Tested.

(b) Section views of coating system before and after endurance testing for 30 minutes at 19.6×10^6 watts/meter^2 (12 Btu/(in.^{2})(sec)).

Figure 11. - Coating system structure changes of sample 4:D (Mo sublayer/nichrome middle layer/Al_2O_3 outer layer) resulting from hydrogen plasma testing. Original photomicrograph, X250.

(a) Face view of coating system sample after step testing to 9.8×10^6 watts/meter^2 (6 Btu/(in.^{2})(sec)). Original photograph, X3.

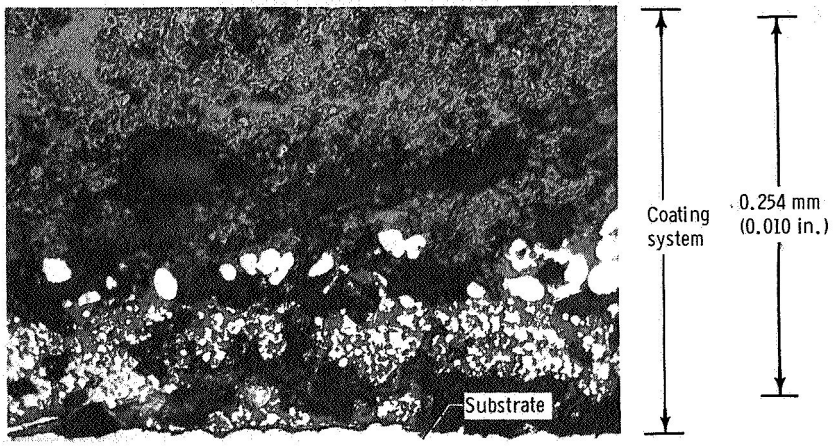

(b) Section view of untested coating system. Original photomicrograph, X250.

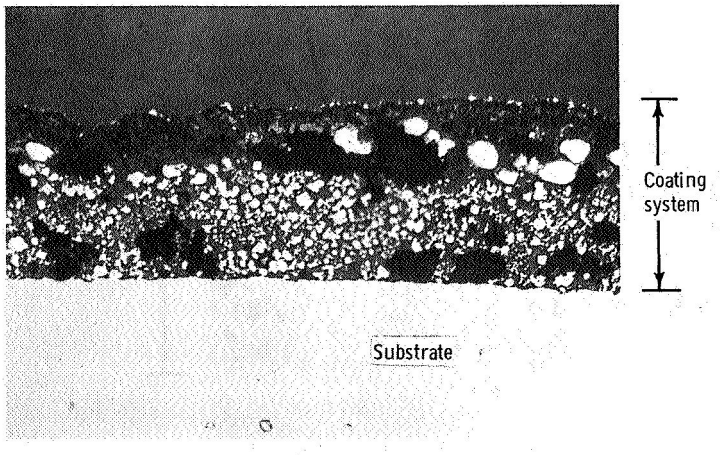

(c) Section view of coating system step tested to 9.8×10^6 watts/meter^2 (6 Btu/(in.^{2})(sec)). Original photomicrograph, X250.

Figure 12. - Coating system surface and structure changes of sample 4:E (Mo sublayer/nichrome middle layer/Al_2O_3 outer layer) resulting from hydrogen plasma testing.

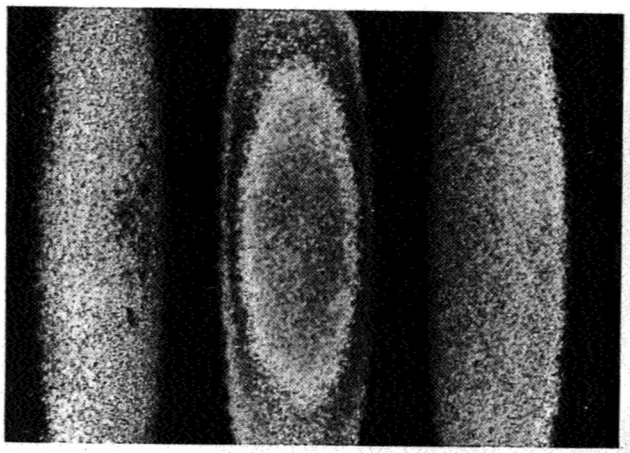

(a) Face view of coating system sample after endurance testing for 30 minutes at 19.6×10^6 watts/meter^2 (12 Btu/in.^{2})(sec)). Original photograph, X3.

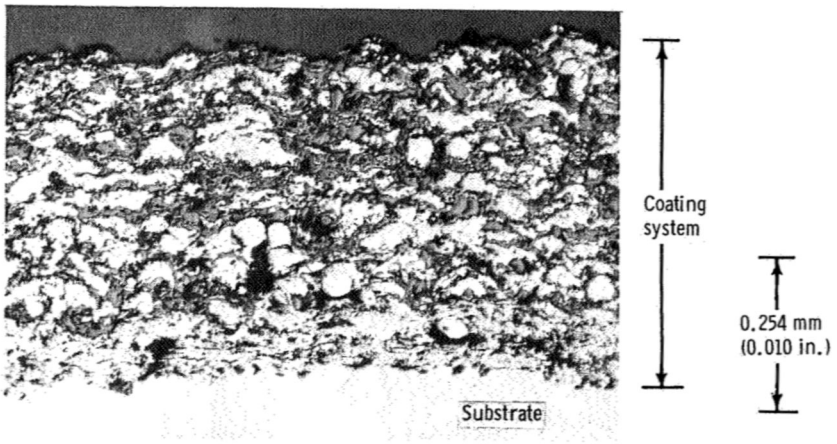

(b) Section of untested coating system. Original photomicrograph, X100.

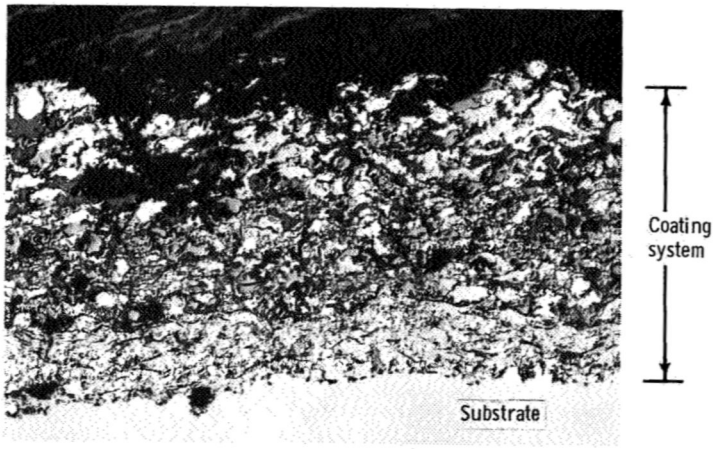

(c) Section view of coating system endurance tested for 30 minutes at 19.6×10^6 watts/meter^2 (12 Btu/in.^{2})(sec)). Original photomicrograph, X100.

Figure 13. - Coating system surface and structure changes of sample 6:C (W-NICORO 80 sublayer/W-ZrO_2-Cu outer layer) resulting from hydrogen plasma testing.

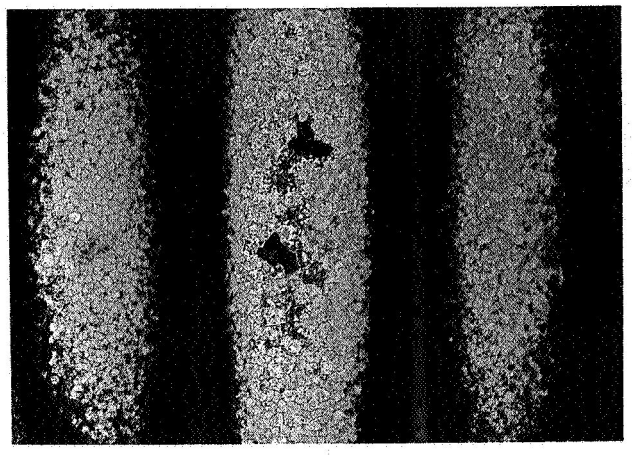

(a) Face view of coating system sample after endurance testing for 30 minutes at 19.6×10^6 watts/meter^2 (12 Btu/in.^{2})(sec)). Original photograph, X3.

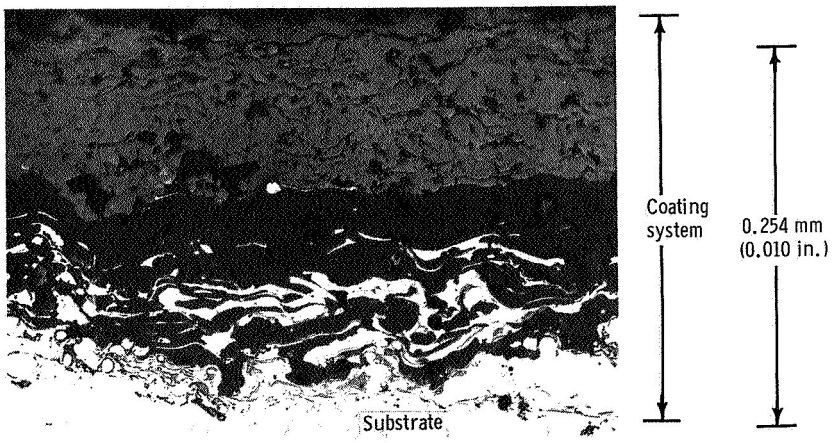

(b) Section view of untested coating system. Original photomicrograph, X250.

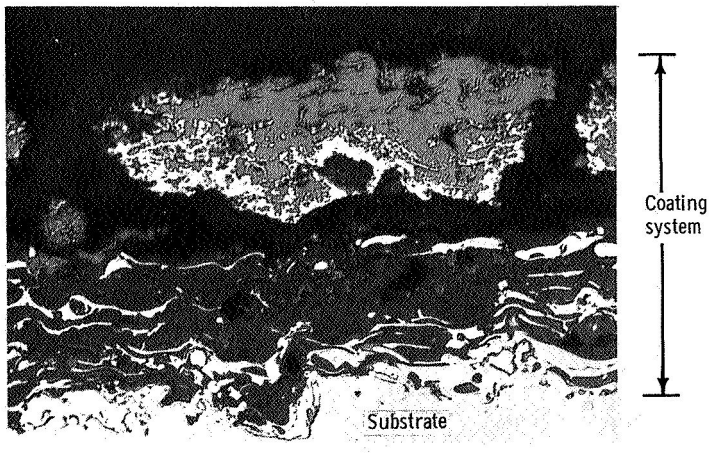

(c) Section view of coating system endurance tested for 30 minutes at 19.6×10^6 watts/meter^2 (12 Btu/in.^{2})(sec)). Original photomicrograph, X250.

Figure 14. - Coating system surface and structure changes of sample 7:D (nichrome sublayer/nichrome-Al_2O_3 grading/ZrO_2 outer layer) resulting from hydrogen plasma testing.

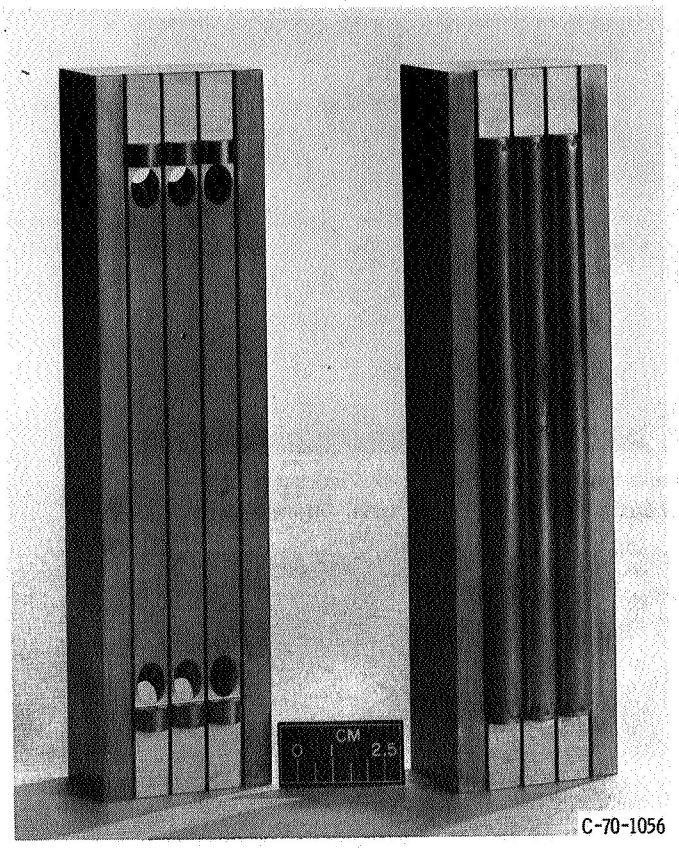

Figure 15. - Heat-flux-meter block before and after fitting of coolant tube shells. Center shell is slotted for thermocouples.

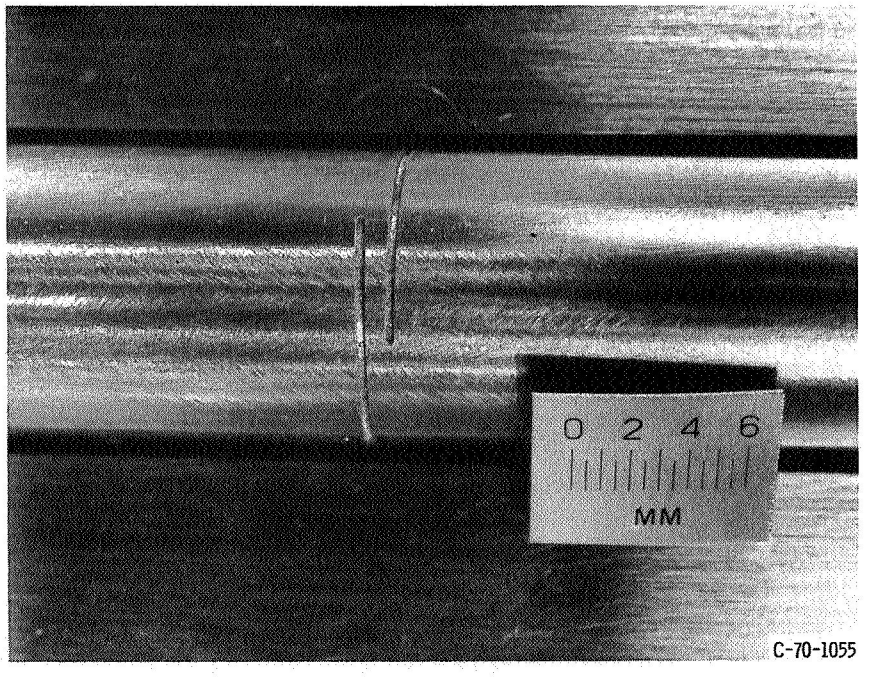

Figure 16. - Enlarged view of center heat-flux-meter tube shell, showing thermocouple slots.

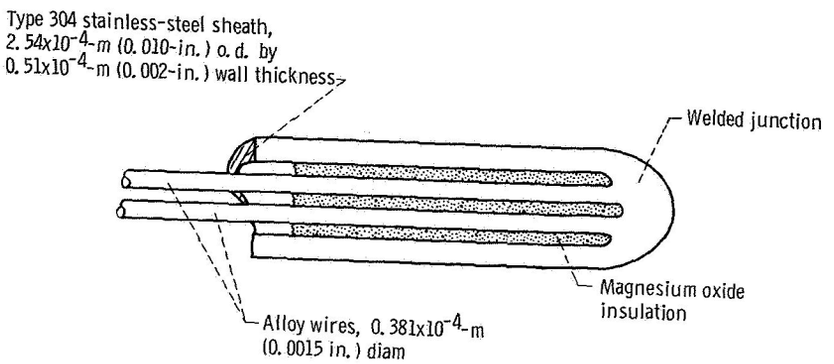

Figure 17. - Details of heat-flux-meter Chromel-Alumel thermocouple assembly.

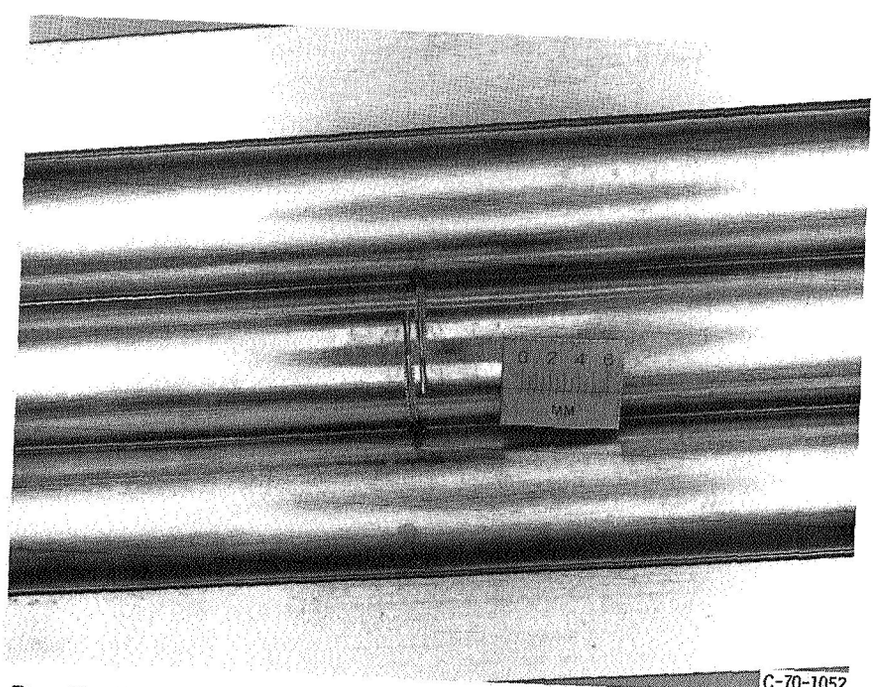

Figure 18. - Thermocouples in place in heat-flux-meter center coolant tube shell prior to assembly brazing.

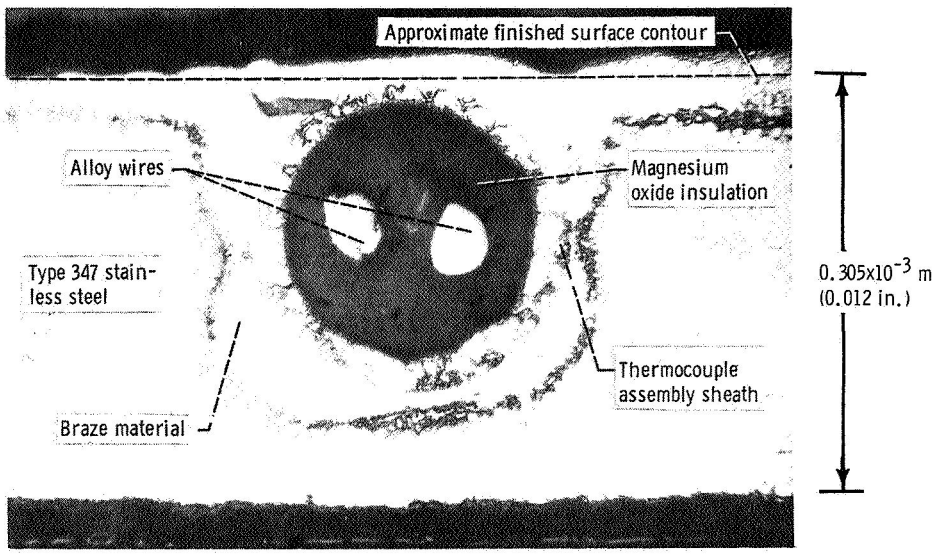

Figure 19. - Photomicrograph (originally X175) of section of 0.254x10^{-3}-meter (0.010-in.) diameter thermocouple assembly installed in 0.305x10^{-3}-meter (0.012-in.) thick type 347 stainless-steel wall. Section was made immediately behind thermocouple junction.

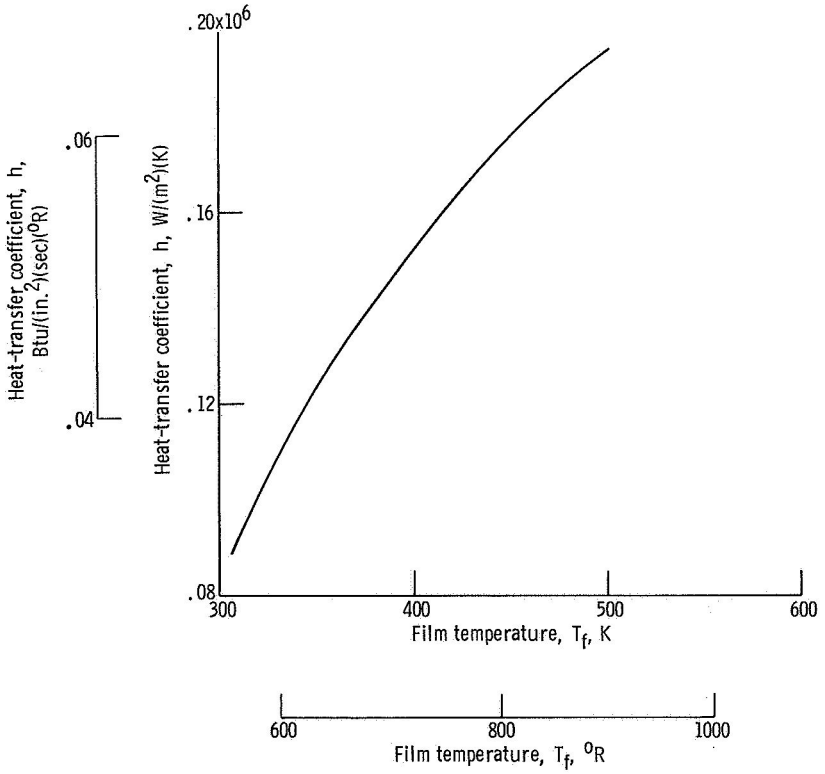

Figure 20. - Internal heat-transfer coefficient of heat-flux-meter coolant tube, as a function of film temperature. Velocity of water, 26.274 meters/second (1034 in./sec); temperature of water, 305.25 K (550^0 R).

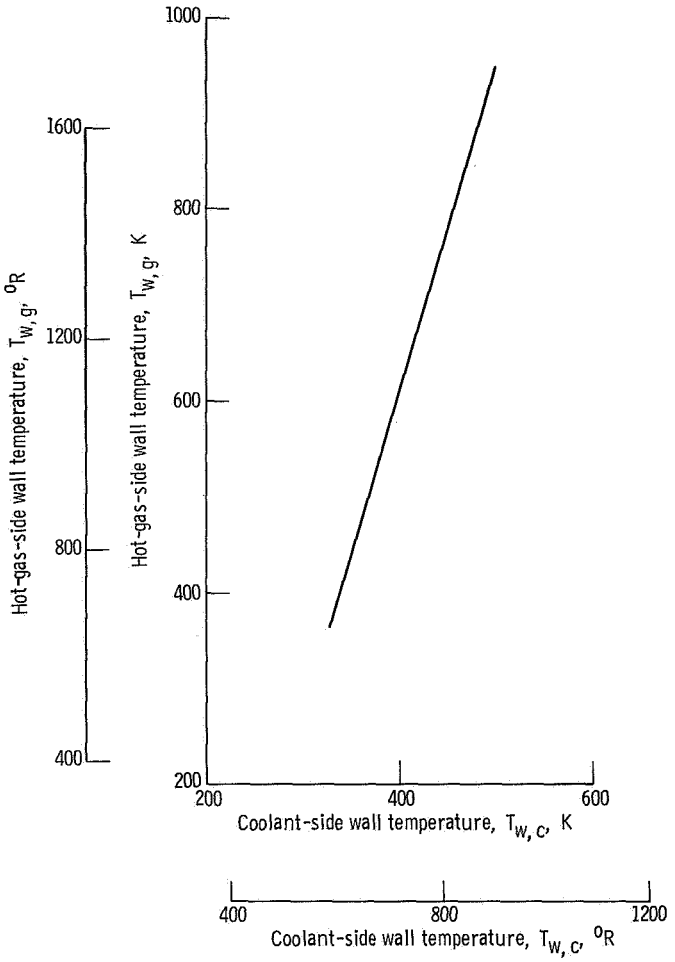

Figure 21. - Hot-gas-side wall temperature of heat-flux-meter coolant tube, as function of coolant-side wall temperature. Velocity of water, 26.274 meters/second (1034 in./sec); temperature of water, 305.25 K (550° R).

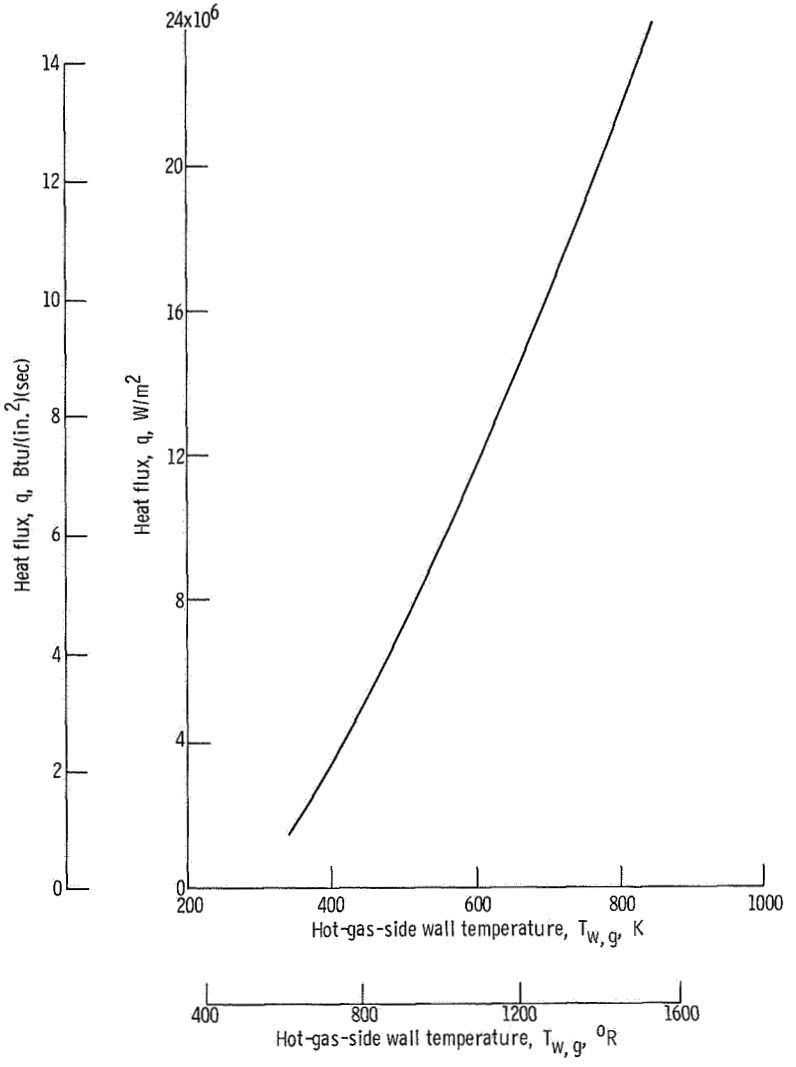

Figure 22. - Heat-flux to heat-flux meter as function of tube hot-gas-side wall temperature. Velocity of water, 26.274 meters/second (1034 in./sec); temperature of water, 305.25 K (550^0 R).

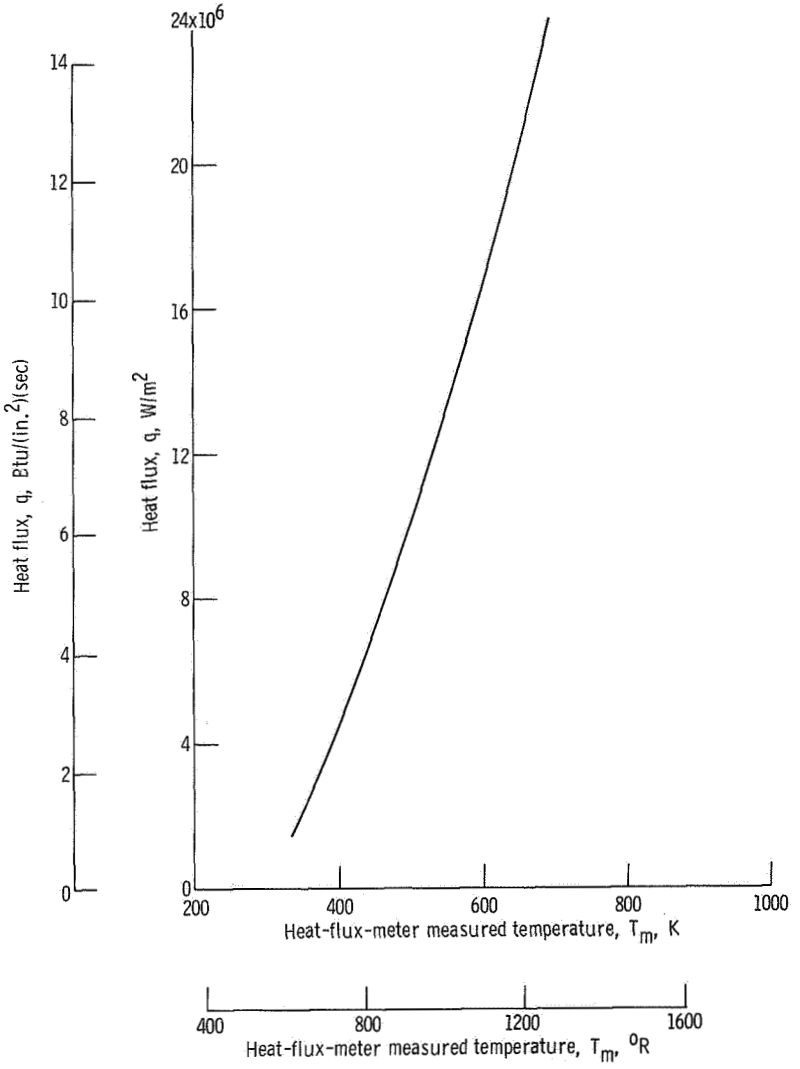

Figure 23. - Heat flux to heat-flux meter as function of measured temperature. Velocity of water, 26.274 meters/second (1034 in./sec); temperature of water, 305.25 K (550^0 R).

"The aeronautical and space activities of the United States shall be conducted so as to contribute . . . to the expansion of human knowledge of phenomena in the atmosphere and space. The Administration shall provide for the widest practicable and appropriate dissemination of information concerning its activities and the results thereof."

—NATIONAL AERONAUTICS AND SPACE ACT OF 1958

NASA SCIENTIFIC AND TECHNICAL PUBLICATIONS

TECHNICAL REPORTS: Scientific and technical information considered important, complete, and a lasting contribution to existing knowledge.

TECHNICAL NOTES: Information less broad in scope but nevertheless of importance as a contribution to existing knowledge.

TECHNICAL MEMORANDUMS: Information receiving limited distribution because of preliminary data, security classification, or other reasons.

CONTRACTOR REPORTS: Scientific and technical information generated under a NASA contract or grant and considered an important contribution to existing knowledge.

TECHNICAL TRANSLATIONS: Information published in a foreign language considered to merit NASA distribution in English.

SPECIAL PUBLICATIONS: Information derived from or of value to NASA activities. Publications include conference proceedings, monographs, data compilations, handbooks, sourcebooks, and special bibliographies.

TECHNOLOGY UTILIZATION PUBLICATIONS: Information on technology used by NASA that may be of particular interest in commercial and other non-aerospace applications. Publications include Tech Briefs, Technology Utilization Reports and Technology Surveys.

Details on the availability of these publications may be obtained from:

SCIENTIFIC AND TECHNICAL INFORMATION OFFICE

NATIONAL AERONAUTICS AND SPACE ADMINISTRATION

Washington, D.C. 20546